8-16-2012 12:00 AM

Biomechanical Modeling for Lung Tumor Motion Prediction during Brachytherapy and Radiotherapy

Zahra Shirzadi
The University of Western Ontario

Supervisor
Dr. Abbas Samani
The University of Western Ontario

Graduate Program in Biomedical Engineering

A thesis submitted in partial fulfillment of the requirements for the degree in Master of Engineering Science

© Zahra Shirzadi 2012

Biomechanical Modeling for Lung Tumor Motion Prediction during Brachytherapy and Radiotherapy

(Spine title: Biomechanical Modeling for Lung Tumor Motion Prediction)

(Thesis format: Integrated Article)

by

Zahra Shirzadi

Graduate Program in Biomedical Engineering

A thesis submitted in partial fulfillment
of the requirements for the degree of
Master of Engineering Science

The School of Graduate and Postdoctoral Studies
The University of Western Ontario
London, Ontario, Canada

THE UNIVERSITY OF WESTERN ONTARIO
School of Graduate and Postdoctoral Studies

CERTIFICATE OF EXAMINATION

Supervisor   Examiners

_____   _____
Dr. Abbas M. Samani   Dr. James Johnson

Supervisory Committee
                                                        _____
                                                        Dr. James C. Lacefield

_____
Dr. Hanif M. Ladak   _____
                                                        Dr. Stewart Gaede

_____
Dr. Grace Parraga

The thesis by

Zahra Shirzadi

entitled:

**Biomechanical Modeling for Lung Tumor Motion Prediction
during Brachytherapy and Radiotherapy**

is accepted in partial fulfillment of the
requirements for the degree of
Master of Engineering Science

_____   _____
            Date   Chair of the Thesis Examination Board

ii

Abstract

A novel technique is proposed to develop a biomechanical model for estimating lung's tumor position as a function of respiration cycle time. Continuous tumor motion is a major challenge in lung cancer treatment techniques where the tumor needs to be targeted; e.g. in external beam radiotherapy and brachytherapy. If not accounted for, this motion leads to areas of radiation over and/or under dosage for normal tissue and tumors. In this thesis, biomechanical models were developed for lung tumor motion prediction in two distinct cases of lung brachytherapy and lung external beam radiotherapy. The lung and other relevant surrounding organs geometries, loading, boundary conditions and mechanical properties were considered and incorporated properly for each case. While using material model with constant incompressibility is sufficient to model the lung tissue in the brachytherapy case, in external beam radiation therapy the tissue incompressibility varies significantly due to normal breathing. One of the main issues tackled in this research is characterizing lung tissue incompressibility variations and measuring its corresponding parameters as a function of respiration cycle time. Results obtained from an ex-vivo porcine deflated lung indicated feasibility and reliability of using the developed biomechanical model to predict tumor motion during brachytherapy. For external beam radiotherapy, in-silico studies indicated very significant impact of considering the lung tissue incompressibility on the accuracy of predicting tumor motion. Furthermore, ex-vivo porcine lung experiments demonstrated the capability and reliability of the proposed approach for predicting tumor motion as a function of cyclic time. As such, the proposed models have a good potential to be incorporated effectively in computer assisted lung radiotherapy treatment systems.

Keywords

Co-Authorship Statement

The material presented in chapter 2 of the thesis has been published in: Z. Shirzadi, A.S. Naini, A. Samani, "Lung tumor motion prediction during lung brachytherapy using finite element model," *Proceeding of SPIE Medical Imaging 2012: Image-Guided Procedures, Robotic Interventions, and Modeling*, San Diego, California, USA, Vol. 8316, 83160I, 2012.

For this work, I performed experimental work including setup, data acquisition and analysis in addition to image processing with Dr. Sadeghi Naini's assistance. I also wrote the manuscript. Dr. Samani led the project by defining the research theme, providing guidance. He also edited the manuscript and replied to reviewers' critique.

The Material presented in chapter 3 of the thesis has been submitted to the *Journal of Medical Physics* as: Z. Shirzadi and A. Samani, "Towards in-vivo lung's tissue incompressibility characterization for tumor motion predication during lung cancer radiotherapy".

For this work, I performed experimental work including setup, data acquisition and analysis in addition to image processing. I also wrote the manuscript with help from my supervisor Dr. Samani who led the project by defining the research theme, providing guidance and editing the manuscript.

Dedication

I would like to dedicate my thesis to my loving parents for their unconditional love, support and encouragement throughout my life and studies.

To "**my mother**" who has guided me in every moment of my life,

and

To "**my father**" who has taught me to be patient and hard-working to achieve big ambitions in life.

Acknowledgments

Table of Contents

List of Tables

List of Figures

List of Appendices

Chapter 1

Introduction

1.1. Motivation and Literature review

According to the American Cancer Society statistics, lung cancer accounts for more deaths than any other cancer in both men and women [1,2]. In 2011, 14% of cancer incidences was reported for lung cancer while 27% of cancer-related deaths occurred due to lung cancer in the same year. On the other hand, the 1-year survival rate of lung cancer is 43% ; However, its 5-year survival rate is only 16% which is very low compared to the 5-year survival rate of around 90% reported for breast cancer and 99.6% reported for prostate cancer [1]. It is worth mentioning that prostate cancer (29%) and breast cancer (30%) are the most prevalent cancers among men and women, respectively [1,2]. This statistics indicates that methods currently used to treat lung cancer are very far from being sufficiently effective.

Current lung cancer treatment methods include surgery, chemotherapy and external beam radiation therapy or a combination of these techniques. These methods are selected based on the lung cancer type and stage [1]. Surgical resection which involves removing cancerous tissue from normal tissue is not a viable treatment method for patients with poor pulmonary system. Since lung cancer patients usually suffer from other lung diseases, they are not deemed effective for restoring health after surgery. While involving substantial side effects, chemotherapy, on the other hand, may lead to successful outcome for patients in the early stages of cancer[1]. External beam radiation therapy, an alternative treatment technique, is commonly employed for lung cancer therapy by itself or as a complement with chemotherapy and surgery [1,2,3]. The high morbidity rate related to this technique stems from areas of normal tissue overdosage and/or cancerous

tissue underdosage. The radiation beam power and diameter as well as the number of radiation times the patient should undergo are determined by a medical physicist preoperatively. This is done based on a 3D image such as a 3D CT set obtained by averaging a 4D CT sequence[3]. What causes areas of overdosage and/or underdosage is that since the lung moves and deforms during the radiation procedure, a single image is not sufficient to decide how the tumor should be targeted as targeting in this context requires tumor motion compensation [3,4,5,6,7]. A crude method to compensate for such motion to ensure sufficient radiation involves increasing the tissue volume to be irradiated. Using such technique leads to substantial radiation overdosage of healthy tissue which may damage the tissue and further deteriorate the pulmonary function given the number of times radiation needs to be repeated.

Brachytherapy is a novel cancer treatment method in which several small radioactive seeds are directly implanted within the cancerous tissue using needle. These seeds will remain within the tissue permanently to eradicate the cancer cells over time [8,9,10].Brachytherapy has been clinically employed for brain and prostate cancer treatment [9,10]; however, it has not yet been developed for lung cancer clinical treatment although it has a good potential to be applied and reduce this disease's morbidity rate [8,11,12,13]. In brachytherapy, a dosimetry plan which indicates the radioactive seeds spatial distribution pattern within the cancerous tissue volume is determined preoperatively by a medical physicist. The seeds' placement and alignment are designed such that sufficient radiation is absorbed by the cancerous tissue while absorbed radiation by surrounding normal tissue is negligible [11,12]. As small deviations in the seeds configuration can lead to significant areas of tissue over and/or under radiation dosage, it is critical to minimize deviation from the dosimetry plan throughout seeds placement procedure. As such, lung brachytherapy successful treatment is strongly dependent on accurate radioactive seed implantation based on the determined seed pattern [11,12,13,14].

The major challenge in lung cancer treatment methods where the tumor needs to be targeted, including external beam radiation therapy and brachytherapy, is the constant large tissue deformation and high amplitude tumor movement resulting from breathing.

This effect causes radiation overdosage to the healthy tissue while it may cause radiation under/overdosage to cancerous tissue [3,4,5,7,11,13,14]. A number of techniques including motion-encompassing, respiratory gated, breath-hold, forced shallow-breathing and respiratory-synchronized have been proposed and utilized for management of respiratory motion for a limited number of patients [15]. None of these techniques, however, can be regarded as a general solution for tumor movement management. Issues involved in these techniques include, for example, inability of breath holding of many lung cancer patients in the breath-hold technique and excessive treatment time and energy with the respiratory-synchronized technique. As such, it is highly advantageous to develop a tumor tracking system whereby the location of the tumor can be determined accurately and the radiation beam during external beam radiotherapy or brachytherapy needles would target the cancerous tissue with sufficient accuracy in order to minimize radiation over/under dose absorption. Utilizing such system holds a good potential to ameliorate the outcome of these radiation based treatment techniques for lung cancer treatment and as a result reduce the morbidity rate caused by this disease.

Real-time imaging is a possible tumor tracking system for several applications; however, it is not viable for lung tumor tracking as no suitable imaging modality is currently available to determine the lung tumor location with adequate precision. CT imaging, which has enough accuracy to distinguish cancerous tissue from normal tissue, is associated with harmful ionizing energy given the relatively long time of the therapeutic procedures. Moreover, ultrasound (US) imaging cannot be employed for image guided lung cancer treatment due to air within the lung tissue which leads to significant US image quality decline. MRI is also not suitable for lung imaging as it is not suitable for real-time applications including image guided procedures. Another approach for tumor tracking involves developing a computer-based model of the respiratory system mechanics [3,4,7]. This model is expected to determine tumor location as a function of respiration phase by estimating lung tissue deformation during breathing. A motion tracking system which has the capability of respiration phase determination along with such model can provide tumor location during radiation based procedures in a real-time fashion. Computer-based modeling approaches that can be utilized for tissue deformation

estimation and tumor tracking can be divided in two major categories:1) nonlinear image registration based modeling and 2) tissue biomechanics based modeling [3,6].

1.1.1. Tumor tracking using image registration based techniques

In image registration based techniques, tissue deformation estimation is obtained directly from 4D image data set [3]. In this approach, non-rigid or deformable image registration (DIR) is required, since the lung tissue undergoes large deformations throughout respiration. Kessler utilized image registration of different imaging modalities to quantify their information and to use that information for various purposes including cancer staging, cancer treatment outcome assessment after radiotherapy, etc. Different metrics for registration along with various optimizers were employed in this study to find the best match among images and estimated tissue deformation fields[7]. Coselmon *et al* conducted a similar study. They employed Thin Plate Spline image registration as well as simplex algorithm for optimization. The utilized optimization cost function in their simulations was Mutual Information [16]. Urschler *et al* also obtained lung tissue deformation fields where they determined the lung and diaphragm movement using a non-rigid Thin Plate Spline registration technique. They conducted phantom studies as well as real sheep thorax experiments and assessed the achieved deformation field accuracy using manually identified landmarks [17].Stein *et al* assessed the accuracy and speed of two Demons-based registration methods for quantifying lung tissue deformation by applying them to a dynamic MRI data set [18]. Samant *et al* also proposed a high performance computing technique based on Graphics Processing Unit (GPU) technology to increase the Demons-based DIR process speed and provide it for adaptive radiotherapy [19]. McClelland *et al* employed B-spline image registration along with nonlinear least squares optimization in order to find the correspondence between a 4D CT data set obtained from free breathing cycle and a reference CT image obtained in breath hold situation. In their analysis, a respiratory signal was also considered together with the 4D CT acquisition [20]. Although several DIR approaches were proposed to model different organs' deformation [21,22], these techniques deal with multi-dimensional optimization algorithms and can be prone to errors associated with uniqueness issue.

1.1.2. Tumor tracking using biomechanical modeling

Apart from image-based DIR techniques which were discussed in the previous section, physics based DIR using Finite element method (FEM) has gained attention among researchers in several applications. Courtis *et al* proposed a technique to estimate prostate tissue displacement field resulting from US probe loading using a FE based multimodality DIR [23,24]. Similar studies were conducted to calculate lung tissue deformations using respiration mechanics. In these techniques, the organ geometry required for FE analysis was extracted from corresponding images. Different approaches can be employed to apply required loading to the respective FE model. Landmark displacements obtained from 4D image sequence was considered as loading in a number of studies while surface matching was used in other studies to find sought displacement loading. Although the first approach involves internal tissue structures assessment which may seem more suitable for tumor tracking, the fact that the number of landmarks that can be defined within the tissue is usually small limits the utility of this approach. Zhang *et al* conducted a surface matching FE based DIR to calculate lung tissue deformation field between end exhale to end inhale [25]. Villard *et al*, Eom *et al* and Werner *et al* utilized a similar concept where they considered two phases for respiration: end exhale and end inhale. They applied some force or pressure to the surface of the lung model such that the obtained deformed model is restricted by the final volume of the lung or the chest cavity model [3,26,27]. A lung phantom and 12high resolution 4D CT images of lung cancer patients were investigated in the study conducted by Werner *et al*to assess the accuracy of their proposed technique. In their study, the soft tissue was assumed to be linear elastic, isotropic and homogeneous. In the phantom study, several material properties (Young's modulus and Poisson's ratio) and pressure loading were examined to investigate the mechanical properties impact on the achieved displacement field. They concluded that considering their assumptions and modeling simplifications, various mechanical properties do not have significant effect on the resulting deformation fields. Therefore, for the real patient models, they assumed a Young's modulus and Poisson's ratio based on the phantom study and calculated the errors of different models by comparing landmarks displacements identified by experts [3].

A number of lung respiration FE modeling investigations were performed by Al-Mayah *et al.* Their model is also based on surface matching while they did not apply pressure to the end exhale model. Instead, they considered end inhale image as a reference volume and applied the distance between inhale and exhale surfaces as prescribed displacement boundary conditions to this reference volume. Three simulations were conducted in [5,6] to compare the results; linear elastic material properties without lung-chest cavity contact, Marlow hyperelastic without lung-chest cavity contact and Marlow hyperelastic with lung-chest cavity contact. By comparison of 45 landmarks displacements in these cases, they concluded that accuracy is higher for the model that involved hyperelasticity and contact effect. They also evaluated their model's accuracy by modeling 16 lung cancer patient images for different friction coefficient amounts in lung-chest cavity contact and various lung's Poisson's ratio. The frictionless contact model with a Poisson's ratio of 0.4 led to the smallest error for their model [28]. Moreover, they demonstrated that the homogeneity simplification is a reasonable assumption for lung biomechanical modeling [29]. This was also shown for deflated lung using in-silico phantom studies by Sadeghi Naini *et al* [30].

Tissue intrinsic mechanical properties expressed by its constitutive law are a fundamental element in its FE model. Given the known lung tissue intrinsic nonlinearity combined with geometric nonlinearity exhibited by the lung under physiological conditions, incorporating hyperelastic constitutive law is necessary for FE modeling. Hyperelastic constitutive law development is based on strain energy functions developed for this purpose. Various strain energy functions have been utilized in developing tissue hyperelastic models. These include polynomial, Yeoh, Marlow and Veronda-Westmann models. Once the strain energy function is selected, the following equation can be derived as the tissue constitutive law:

$$\sigma = \frac{2}{J} DEV\left[\left(\frac{\partial U}{\partial \bar{I}_1} + \frac{\bar{I}_1 \partial U}{\partial \bar{I}_2}\right)\bar{B} - \frac{\partial U}{\partial \bar{I}_2}\bar{B}.\bar{B}\right] - PI$$

$$\bar{B} = \bar{F}.\bar{F}^T, \quad \bar{F} = J^{-\frac{1}{3}}.F, \quad \bar{I}_i = J^{-\frac{2}{3}}.I_i, \text{ and } J = \det(F)$$

where in these equations σ is the stress, *DEV* is the deviatoric part of stress tensor, *U*, *P* and *F* are strain energy, hydrostatic pressure and deformation gradient tensor, respectively. I_i represent the strain invariants and *I* is the identity matrix [31].

1.2. Objective

The investigations discussed in the previous section confirm the suitability of FEM for developing respiration biomechanical models for tumor tracking. The goal of this study is to develop a biomechanical model capable of predicting lung's tumor position with high accuracy as a function of respiration time. Specifically, we aim to achieve an accuracy of within 1mm.This is expected to improve the outcome of radiation based lung cancer treatment procedures by accurately targeting the tumor during respiration leading to minimization of radiation overdose or underdose. In the proposed FEM model, patient specific geometries of the lung, chest wall and diaphragm can be extracted from the patient's preoperative CT image. This image is segmented before the model's 3D FE mesh is generated. In clinical applications, this processing part can be conducted preoperatively while the model's boundary conditions including the chest cavity and diaphragm configuration are required to be determined intraoperatively. To extract this information, a limited number of fiducial markers can be placed on the patients' chest. These markers can be tracked by means of an optical or electromagnetic tracking system. The markers' position data can be then input to the FE model as prescribed displacements boundary conditions. We expect that using this system leads to tumor tracking during respiration in real-time manner.

1.2.1. Tumor tracking during brachytherapy procedure

The first study conducted for this thesis involves tumor tracking during lung brachytherapy. As mentioned before, the major challenge in lung cancer treatment using brachytherapy is constant tumor motion as a result of tissue deformation due to respiration. To minimize the amount of lung tissue deformation and tumor movement, the lung which is under the procedure can be deflated by blocking its major airway. However, since respiration continues with the other lung, continual diaphragm displacement causes significant tumor motion in the lung under seeds' placement

procedure. Therefore, to avoid deviation from the dosimetry plan and tissue over/under radiation dosage, tumor motion tracking is critical.

The geometry of the deflated lung is a prerequisite for FE modeling which we proposed for tumor tracking during respiration. This geometry can be extracted with sufficient accuracy based on the technique described in [32]. Moreover, the loading in this continuum mechanics problem is diaphragm displacement which we assume as rigid contact problem, since the diaphragm muscle thickness is significant while it is much stiffer than the lung tissue as the diaphragm's Young's modulus is reported to be between 100kPa and 5MPa [16,33,34] while the lung tissue Young's modulus is reported at 0.1kPa to 4kPa in different studies [3,5,6].Chest wall contact problem modeling is not necessary in this case since the deflated lung volume is smaller than the normal lung, hence contact development with the chest wall is unlikely. After FE analysis, the 3D tumor motion trajectory components are calculated from the obtained displacements field as a function of time during respiration. For the purpose of validation, this tumor motion trajectory was then compared to the tumor movement obtained from an ex-vivo experiment which was conducted under similar conditions considered in the FE simulation. This comparison demonstrated a good agreement between the experimental and simulation results. Furthermore, analysis was performed to evaluate the sensitivity of lung tumor motion estimation to variations of the lung tissue mechanical properties. This investigation was conducted by varying each coefficient of Yeoh hyperelastic material model, which was considered in the proposed FEM, by up to±20%.These sensitivity analysis confirmed the robustness of the proposed technique for tumor motion tracking with respect to ±20% deviation from the hyperelastic parameters obtained by conducting ex-vivo experiments described in [35].

1.2.2. Tumor tracking during external beam radiotherapy procedure

Another investigation conducted for this thesis tackles the problem of tumor motion tracking in external beam radiotherapy. In this technique, the lung is not deflated, hence respiration motion is much larger compared to brachytherapy. To utilize the proposed FE model for lung tumor tracking during this case, the loading and boundary conditions are

different from those of brachytherapy. Given that the airway is not blocked in this case, normal breathing mechanism and lung volume variation need to be modeled.

Lung model volume variation [36,37,38] is simulated by applying negative pressure to the model surface. Moreover, the lung-chest cavity contact should be incorporated in this analysis as the displacements boundary condition. Apart from geometry, loading and boundary conditions which are required components of FE modeling, knowledge of accurate and reliable mechanical properties of lung tissue has been always a concern in the respiratory system biomechanical modeling. These parameters are deemed to have significant variation due to air content variation within the lung during respiration. To consider these parameter variations, one approach is to idealize lung tissue as a biphasic material including soft tissue and air phases. This, however, causes modeling and parameters measurement complexities.

A more practical approach, which we utilized in our model, is considering variable mechanical parameters. The goal of this part of research is to characterize lung tissue incompressibility parameter variation as a function of time during respiration. Incompressibility parameter is expected to vary significantly as a result of air content variation and more importantly, it is predicted that its variation has noticeable impact on the tumor motion.

First, the advantage of using varying incompressibility parameter over a constant incompressibility parameter in tumor movement estimation throughout respiration cycle was investigated by conducting an in-silico phantom study. Several simulations in the in-silico phantom study, including linear elastic and Marlow hyperelastic material properties, indicate the importance of using variable incompressibility parameter to obtain tumor motion characteristics. After establishing the importance of modeling tissue incompressibility variation during respiration, a novel technique was developed to characterize this variation. For this purpose, an optimization inverse problem framework [39] was used where the tissue incompressibility parameter was varied systematically until the maximum similarity between acquired 4D image sequence and their counterpart obtained from FE analysis was achieved. Utilizing this technique, incompressibility

parameter function of respiration time cycle was calculated for the inspiration phase of breathing.

Throughout this analysis, a 4D CT image sequence of a ventilated lung was used. Moreover, for validation, the calculated incompressibility parameter function was employed to model the expiration phase of breathing using the images related to the exhale phase for validation. Image similarity measures [40],which were used to evaluate the results, demonstrated that the obtained incompressibility parameter function obtained from the inspiration phase image data can predict the exhale phase images with high accuracy. It was also shown that using such function for incompressibility parameter increases the tumor motion estimation accuracy lead in to a precise lung tumor tracking system required for more effective radiotherapy procedure.

1.3. Thesis Outlines

The abovementioned thesis objective has been described in three following chapters. Chapter 2 is dedicated to lung's tumor motion predication during lung brachytherapy using the FEM proposed for deflated lung modeling. The tumor trajectory components and the sensitivity analysis results as well as experimental validation are included in this chapter. In chapter 3, lung's tissue incompressibility characterization technique is described while its importance is also demonstrated. The thesis conclusions and discussion are given in Chapter 4. In this chapter, the presented materials in chapters 2 and 3 are summarized and possible future directions are declared.

References

[1] American cancer society, http://www.cancer.org/Research/CancerFactsFigures/index

[2] A. Jemal, F. Bray, M.M. Center, J. Ferlay, E. Ward, D. Forman, "Global cancer statistics," CA Cancer Journal for Clinicians 61, 69-90 (2011).

[3] R. Werner, J. Ehrhardt, R. Schmidt, H. Handels, "Patient-specific finite element modeling of respiratory lung motion using 4D CT image data," Med. Phys. 36, 1500-1511 (2009).

[4] G. Li, D. Citrin, K. Camphausen, B. Mueller, C. Burman, B. Mychalczak, R.W. Miller, Y. Song, "Advances in 4D medical imaging and 4D radiation therapy," Technol. Cancer. Res. Treat. 7, 67-81 (2008).

[5] A. Al-Mayah, J. Moseley, K.K. Brock, "Contact surface and material nonlinearity modeling of human lungs," Phys. Med. Biol. 53, 305-317 (2008).

[6] A. Al-Mayah, J. Moseley, M. Velec, K.K. Brock, "Sliding characteristic and material compressibility of human lung: Parametric study and verification," Med. Phys. 36, 4625-4633 (2009).

[7] M.L. Kessler, "Image registration and data fusion in radiation therapy," Br. J. Radiol. 79 Spec No 1, S99-108 (2006).

[8] A.W. Lin, A.L. Trejos, R.V. Patel, R. Malthaner, "Robot-assisted minimally invasive brachytherapy for lung cancer," Telesurgery, Chap. 4, pp. 33-52 (2007).

[9] N. Tselis, C. Kolotas, G. Birn, S. Röddiger, I. Filipowicz, M. Kontova, G. Fountzilas, P. Selviaridis, D. Baltas, R. Heyd, G. Anagnostopoulos, N. Zamboglou, "CT-guided interstitial HDR brachytherapy for recurrent glioblastomamultiforme: Long-term results," Strahlentherapie und Onkologie 183, 563-570 (2007).

[10] S. Nag, J.P. Ciezki, R. Cormack, S. Doggett, K. DeWyngaert, G.K. Edmundson, R.G. Stock, N.N. Stone, Y. Yu, M.J. Zelefsky, "Intraoperative planning and evaluation of permanent prostate brachytherapy: Report of the American Brachytherapy Society," International Journal of Radiation Oncology Biology Physics 51, 1422-1430 (2001).

[11] A.L. Trejos, A.W. Lin, M.P. Pytel, R.V. Patel, R.A. Malthaner, "Robot-assisted minimally invasive lung brachytherapy," International Journal of Medical Robotics and Computer Assisted Surgery 3, 41-51 (2007).

[12] V.W.K. Ng, J.E.S. Husband, V.M.C. Nicolson, I. Minty, A. Bamias, "CT evaluation of treatment response in advanced gastric cancer," Clin. Radiol.51, 214-220 (1996).

[13] A.L. Trejos, R.V. Patel, R. Malthaner, "A device for robot-assisted minimally-invasive lung brachytherapy," presented at 2006 Conference on International Robotics and Automation, 15-19 May 2006.

[14] A.S. Naini, R.V. Patel, A. Samani, "A totally deflated lung's CT image construction by means of extrapolated deformable registration," presented at Progress in Biomedical Optics and Imaging, SPIE medical Imaging, 10-16 Feb. 2011.

[15] P.J. Keall, G.S. Mageras, J.M. Balter, R.S. Emery, K.M. Forster, S.B. Jiang, J.M. Kapatoes, D.A. Low, M.J. Murphy, B.R. Murray, C.R. Ramsey, M.B. Van Herk, S.S. Vedam, J.W. Wong, E. Yorke, "The management of respiratory motion in radiation oncology report of AAPM Task Group 76," Med. Phys. 33, 3874-3900 (2006).

[16] M.M. Coselmon, J.M. Balter, D.L. McShan, M.L. Kessler, "Mutual information based CT registration of the lung at exhale and inhale breathing states using thin-plate splines," Med. Phys. 31, 2942-2948 (2004).

[17] M. Urschler and H. Bischof, "Assessing breathing motion by shape matching of lung and diaphragm surfaces," presented at Physiology, Function, and Structure from Medical Images, SPIE medical Imaging, 13-15 Feb. 2005.

[18] D. Stein, R. Tetzlaff, I. Wolf, H.-. Meinzer, "Accuracy of non-rigid registration for local analysis of elasticity restrictions of the lungs," presented at Visualization, Image-Guided Procedures, and Modeling, SPIE medical Imaging, 8-10 Feb. 2009.

[19] S.S. Samant, J. Xia, P. Muyan-Ozcelik, J.D. Owens, "High performance computing for deformable image registration: towards a new paradigm in adaptive radiotherapy," Med. Phys. 35, 3546-53 (2008).

[20] J.R. McClelland, J.M. Blackall, S. Tarte, A.C. Chandler, S. Hughes, S. Ahmad, D.B. Landau, D.J. Hawkes, "A continuous 4D motion model from multiple respiratory cycles for use in lung radiotherapy," Med. Phys. 33, 3348-58 (2006).

[21] W.R. Crum, T. Hartkens, D.L. Hill, "Non-rigid image registration: theory and practice," Br. J. Radiol. 77 Spec No 2, S140-53 (2004).

[22] J.B.A. Maintz and M.A. Viergever, "A survey of medical image registration," Med. Image Anal.2, 1-36 (1998).

[23] P. Courtis and A. Samani, "Biomechanical registration of prostate images using statistical shape models," presented at Physiology, Function, and Structure from Medical Images, SPIE medical Imaging, 12 Feb. 2006.

[24] P. Courtis and A. Samani, "Detecting mechanical abnormalities in prostate tissue using FE-based image registration," presented at 10th Int. Conf. Med. Image Comput. Assist. Interv. (MICCAI), 29 Oct.-2 Nov. 2007.

[25] T. Zhang, N.P. Orton, T.R. Mackie, B.R. Paliwal, "Technical note: A novel boundary condition using contact elements for finite element deformable image registration," Med. Phys. 31, 2412-2415 (2004).

[26] P.-. Villard, M. Beuve, B. Shariat, V. Baudet, F. Jaillet, "Simulation of lung behavior with finite elements : Influence of bio-mechanical parameters," presented at 3rd International Conference on Medical Information Visualization - BioMedical Visualization, MediVis, 5-7 July 2005.

[27] J. Eom, C. Shi, X.G. Xu, S. De, "Modeling respiratory motion for cancer radiation therapy based on patient-specific 4DCT data," Lect. Notes Comput. Sci. 5762 LNCS, 348-355 (2009).

[28] A. Al-Mayah, J. Moseley, M. Velec, K. Brock, "Effect of friction and material compressibility on deformable modeling of human lung," Lect. Notes Comput.Sci.5104 LNCS, 98-106 (2008).

[29] A. Al-Mayah, J. Moseley, M. Velec, S. Hunter, K. Brock, "Deformable image registration of heterogeneous human lung incorporating the bronchial tree," Med. Phys. 37, 4560-71 (2010).

[30] A.S. Naini, R.V. Patel, A. Samani, "Effects of deflated lung's geometry simplifications on the biomechanical model of its tumor motion: A phantom study," presented at Biomedical Optics and Imaging, SPIE Medical Imaging 10-16 Feb. 2011.

[31] H. Mehrabian, G. Campbell, A. Samani, "A constrained reconstruction technique of hyperelasticity parameters for breast cancer assessment," Phys. Med. Biol. **55**, 7489-7508 (2010).

[32] A.S. Naini, G. Pierce, Ting-Yim Lee, R.V. Patel, A. Samani, "CT image construction of a totally deflated lung using deformable model extrapolation," Med. Phys. 38, 872-83 (2011).

[33] J. Saade, A.-.Didier, R. Buttin, J.-.Moreau, M. Beuve, B. Shariat, P.-. Villard, "A preliminary study for a biomechanical model of the respiratory system," presented at International Conference on Computer Vision Theory and Applications, 17-21 May 2010.

[34] E. Promayon and P. Baconnier, "A 3D discrete model of the diaphragm and human trunk," ESAIM Proceedings 23, 66-77 (2008).

[35] A.S. Naini, R.V. Patel, A. Samani, "Measurement of lung hyperelastic properties using inverse finite element approach," IEEE Transactions on Biomedical Engineering 58, 2852-9 (2011).

[36] A.P. Santhanam, "Modeling, simulation and visualization of 3D lung dynamics," Electronic Dissertation Repository 1301, http://etd.fcla.edu/CF/CFE0001301, (2006).

[37] L. Sherwood, "Human physiology: From cells to systems," Cengage Learning 7, 464-470, (2008).

[38] A.S. Naini, Ting-Yim Lee, R.V. Patel, A. Samani, "Estimation of lung's air volume and its variations throughout respiratory CT image sequences," IEEE Transactions on Biomedical Engineering 58, 152-8 (2011).

[39] J.C. Lagarias, J.A. Reeds, M.H. Wright, P.E. Wright, "Convergence properties of the Nelder-Mead simplex method in low dimensions," SIAM Journal on Optimization 9, 112-47 (1998).

[40] D.L.G. Hill, P.G. Batchelor, M. Holden, D.J. Hawkes, "Medical image registration," Phys. Med. Biol. 46, 1-45 (2001).

Chapter 2

Lung Tumor Motion Prediction during Lung Brachytherapy using Finite Element Model

(The modified version of the material presented in this chapter has been published in: Z. Shirzadi, A.S. Naini, A. Samani, "Lung tumor motion prediction during lung brachytherapy using finite element model," Proceeding of SPIE Medical Imaging 2012: Image-Guided Procedures, Robotic Interventions, and Modeling, San Diego, California, USA, Vol. 8316, 83160I, 2012.)

2.1. Introduction

Lung cancer is the leading cause of cancer death in both men and women. According to the statistics of the U.S. National Cancer Institute (NCI), 222,520 new cases of lung cancer were reported in United States in the year 2010, while 157,300 lung cancer related deaths occurred in the same year. This statistics indicates that lung cancer mortality rate is very high, which implies that current lung cancer treatment methods suffer from high morbidity rates and/or significant side effects. Surgery is one of the current methods used to treat lung cancer, which has high morbidity rate as it is very invasive. Lung cancer often occurs in elderly people who may not recover from surgery as it involves surgically removing part of a lung lobe, the whole lobe or in some cases even more. External beam radiation therapy is another technique to treat lung cancer. Treatment outcome in this method is affected by continuous tumor motion due to respiration. Not accounted for this motion during the radiation may lead to cancerous tissue radiation underdosagee or the normal tissue radiation overdosage. Chemotherapy is another method for lung cancer treatment. This method has significant side effects and low success rate. Lung

brachytherapy is a novel cancer treatment technique which holds a good potential for effective lung cancer treatment. In this technique, radioactive seeds are directly implanted within the tumor. The radioactive seeds will remain within the tumor permanently to eradicate cancer cells. The aim of applying this minimally invasive technique in lung cancer treatment is to reduce the morbidity rate and side effects compared to those of current treatment methods [1].

In brachytherapy, a dosimetry plan indicating radiation dose distribution is determined preoperatively. In fact, a dosimetry plan represents a seed spatial distribution pattern within the tumor volume. This distribution is determined such that sufficient radiation is applied to the tumor volume in order to destroy cancerous cells while insignificant amount of radiation is accumulated in the surrounding normal tissues. It is important to note that small deviations in seed placement and alignment may lead to significant areas of tissue over and/or under radiation dosage, hence impacting the procedure's treatment success [2,3]. As such, successful treatment with brachytherapy requires minimizing deviation from the determined seed pattern or dosimetry plan. While brachytherapy has been clinically applied in treating brain and prostate cancer, it is yet to be developed for lung cancer treatment due to some challenges [2,3,4].

The major challenge in lung brachytherapy is tumor motion which results from normal lung tissue deformation due to respiration process. This motion can cause very significant tissue radiation over/under dosage [2]. To minimize the motion, the target lung is fully deflated. Nevertheless, significant tumor motion occurs because of the continued diaphragm motion necessary for respiring the other lung. It is noteworthy that a lung brachytherapy procedure may take several minutes, hence it is not possible to deflate both lungs. To minimize tissue over/under radiation dosage, tracking tumor motion is necessary. In general, tumor tracking can be done using preoperative images, or it can be performed using intra-operative image guidance. In lung brachytherapy, preoperative images are not as effective as in brain brachytherapy [5,6]. This lack of effectiveness stems from the fact that preoperative images are obtained while the lung is partially inflated during respiration whereas the lung being treated is almost completely deflated during brachytherapy. Furthermore, US image guidance, which has the potential to be

used during the procedure is far from ideal for lung brachytherapy. This is because, unlike prostate US images [5,7], US images of a deflated lung have poor quality due to small amount of residual air remaining in the deflated lung.

The objective of this study is to develop an alternate technique for tracking lung tumor during brachytherapy. This technique is based on a biomechanical modeling of the deflated lung. In this research, we employ the Finite Element Method (FEM) to model deflated lung's tissue deformation resulting from the diaphragm's contact forces. This is possible as previous work has shown that FE modeling has sufficient accuracy to predict the mechanical behavior of the respiration system [8,9,10,11]. In this study, we utilize the FE tissue displacements results to calculate a 3D trajectory of the tumor motion during a respiration cycle. This trajectory is presented as a function of the diaphragm displacement at each respiration phase. For validation, an experiment involving ex-vivo porcine lung was performed. The tumor motion results of this experiment demonstrated good agreement with the FE simulation results. Moreover, major sources of uncertainties in the lung biomechanical model and resulting tumor motion estimation were investigated in this research. This included uncertainties in the lung tissue hyperelastic properties, which was incorporated in the model by varying the hyperelastic parameters of the lung tissue by up to ±20%. This investigation showed that the proposed FE model is robust.

2.2. Methods

2.2.1. Ex-vivo porcine lung imaging and contact loading

This investigation involved an ex-vivo phantom study which employs the proposed lung biomechanical model. Figure 2.1 shows a block diagram of the process where the biomechanical model of the deflated lung is utilized to determine the motion of a phantom tumor sutured in the ex-vivo lung in conjunction with validation.

A spherical phantom tumor was sutured inside an ex-vivo porcine left lung. This tumor was constructed from gelatin and agar in addition to ~3 mg/ml iodine CT contrast agent such that it had a Hounsfield unit of ~ 200 HU. After its air was sucked out, the lung was scanned using a GE Healthcare Discovery CT 750 HD scanner (Waukesha, WI). A series of 4.0 cm axial field of view sequential adjacent cine scans were performed. Each cine

scan lasted for 6 sec. The CT scanning parameters were 80 kVp, 200 mA, and a gantry rotation period of 0.4 sec. Each cine scan was retrospectively reconstructed to 32×1.25 mm slices and a field of view of 22 cm. Figure 2.2 shows a slice of the deflated lung image which contains the tumor. After scanning, the lung was hung via the trachea using a frame used to apply the contact loading.
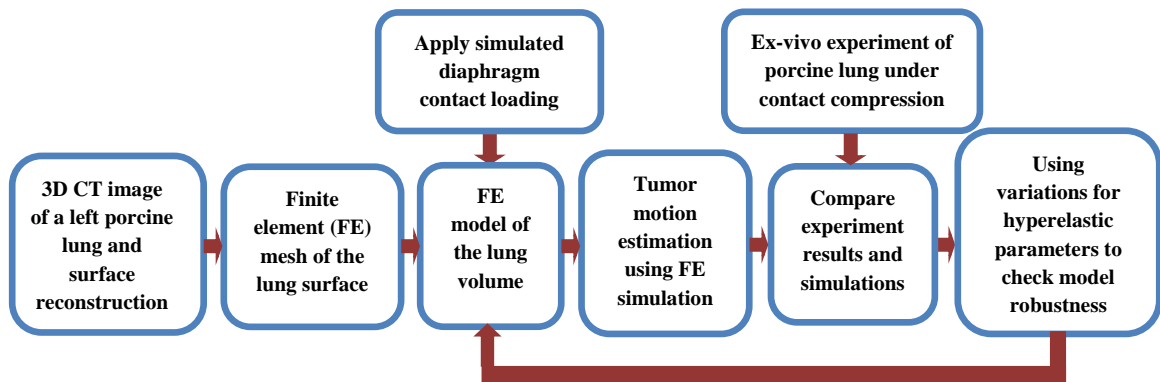
Figure 2.1: Diagram of deflated lung FE modeling as a result of diaphragm movement and validation of the simulations.
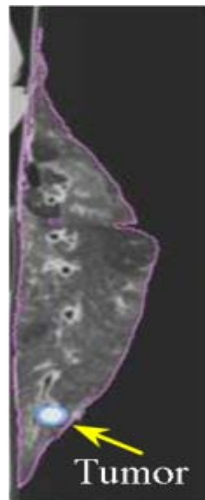
Figure 2.2: A CT image slice of the porcine lung with a phantom tumor segmented using thresholding method.

Figure 2.3: Ex-vivo experiment results of the 25 mm upward contact body displacement. Left: before applying the contact body and right: after applying the contact body.

A small spot on the lung's surface adjacent to the sutured tumor was located and marked using color ink for validation. Next, contact loading, which simulates the diaphragm's loading, was applied to the inferior surface of the lung by pushing it slowly 25 mm upward (in the SI direction) with a cylindrical glass beaker of 115 mm diameter. During loading, a number of photographs were taken to track the marked point motion with respect to the beaker's displacement as shown in Figure 2.3.

2.2.2. Finite element meshing

To construct the ex-vivo porcine deflated lung's FE model, we first generated its FE mesh using the 3D CT scan of the lung that we segmented using a thresholding technique. The thresholding technique was applied to each slice of the lung's CT image using 3D slicer software package [12]. Next, the segmented 2D slices were input through the model maker module of 3D slicer software for surface construction. This was followed by smoothing the lung surface using a Laplacin filter to remove sharp artifacts. Using the resulting smooth surface, the IA-FEMesh open-source software with an elliptical interpolation technique was employed to construct a high quality FE mesh with eight-noded hexahedral elements. With a smaller number of elements compared to tetrahedral element based mesh, using such elements is known to yield high quality mesh leading to accurate FE results. The generated mesh contains 22350 elements and 25603 nodes.

2.2.3. Finite element model

The FE mesh was input into ABAQUS software (*Dassault Systčmes* Simulia Corp., Providenec, RI, USA) for FE analysis. The Yeoh hyperelastic parameters of the lung tissue and linear elastic parameters of tumor were measured by indentation tests in previous studies conducted in our laboratory and input in the model [13]. The Yeoh model is a hyperelastic model usually used for modeling the deformation of nearly incompressible and nonlinear materials. Since the lung is deflated in our model, the tissue is highly incompressible. Furthermore, while undergoing the contact loading the tissue experiences large deformation leading to both geometric and intrinsic nonlinearities. As such, the Yeoh strain energy model is appropriate for modeling the lung tissue. To develop the model, the lung's boundary conditions and contact loading pertaining to the

experiment are required as input. In general lung mechanics, the lung's contact with the chest wall has a major effect; however, in brachytherapy the lung is deflated, hence it is significantly smaller than the chest cavity. Therefore, the free hanging lung in the experiment provides a good simulation of in-vivo lung undergoing brachytherapy as the effect of its contact with the chest wall can be ignored. To provide a fixed boundary condition required in the model, following other researchers, the trachea was fixed to the frame used to hang the lung [14]. It is noteworthy that in brachytherapy the in-vivo lung undergoing the procedure is surgically blocked to prevent respiration. Therefore, similar to the ex-vivo lung in the experiment, it does not involve uniform pressure loading necessary to simulate respiration. The beaker's loading, which causes the tissue to deform, was modeled as a contact problem. It was modeled as a contact surface which pressed upon the lung's inferior surface incrementally by up to 25 mm vertical prescribed boundary conditions [15,16]. The lung's resulting FE contact problem model was analyzed by ABAQUS and the lung's tissue displacements were calculated. This contact problem was simulated under two conditions: frictionless and with friction. In the frictionless contact simulation, the lung tissue was allowed to slip over the beaker's contact surface. Under the friction condition, since the contact friction coefficient was unknown, the coefficient was changed systematically until the best deformation match with the ex-vivo experiment was achieved. It was found that simulation results corresponding to a friction coefficient of 0.32 has the best match; hence it was used for subsequent steps. Deformed lung FE mesh resulting from the 25 mm displacement of the contact body was obtained for further processing.

2.2.4. Mechanical parameters uncertainty assessment

Mechanical properties of the lung tissue are different in different patients, since commonly lung cancer occurs in conjunction with other lung pathology leading to tissue mechanical properties alteration. Hence, it is very important to take this matter into account in order to assess the method's robustness. For this purpose, after FE model construction, to investigate the impact of mechanical properties uncertainties on the tumor motion prediction, we changed each parameter of the hyperelastic model by -20%, -10%, 10% and 20%. For comparing the displacements results, 18 nodes surrounding the

tumor volume were selected. The mean and variance of these nodes' displacements were calculated for each simulation.

2.3. Results

Figure 2.2 shows one slice of the unloaded lung's 3D CT segmented image which contains the tumor. In this figure, the lung and tumor are segmented in different colors, pink and blue, respectively. Figure 2.4 depicts the lung's smoothed surface and the tumor surface which were constructed by 3D slicer software using the segmented lung image. Figure 2.5 shows the FE mesh in which different colors: red, blue and green represent the trachea elements, tumor elements and normal tissue elements, respectively. This figure shows the good quality of the FE mesh which was constructed using hexahedral elements. The normal lung tissue was modeled using the Yeoh model with hyperelastic parameter values of C10=194.4, C20=257.9, and C30=0.0033 Pa [13]. Linear elastic model with a Young modulus of 18 kPa and poison's ratio of 0.49 was used for the tumor. Four stages were considered to track different stages of the respiration cycle, starting from end inspiration and ending to end expiration. Figure 2.6 shows these four stages of the respiration obtained from the simulation. This figure demonstrates displacement components of each element in each phase of the respiration. The 3D trajectory of the tumor was also obtained from ABAQUS and illustrated as a function of the beaker motion which mimics diaphragm movement as shown in Figure 2.7. This figure shows the three displacement components in the 15 simulation frames. This figure also shows that, as a result of the contact caused by moving the cylinder in the SI direction, the tumor has significant displacements in all the three directions. By comparing with the observed displacements of the marked spot on the lung's surface, these results showed good qualitative agreement. The results obtained from investigating the impact of the hyperelastic parameter uncertainties are shown in Tables 2.1 and 2.2 for the first and second parameters, respectively. The error for the third parameter was close to zero. Errors higher than 5% are shown with yellow color. These results indicate that the tumor motion estimation is not significantly sensitive to the lung's uncertainties of hyperelaqstic parameters except in the LR direction which shows a maximum error of ~13%.This implies that FE modeling can predict tumor motion sufficiently accurately by

having only approximate hyperelastic parameters of the lung tissue. Furthermore, Tables 2.1 and 2.2 show that there is a small displacement variation with respect to the first and second Yeoh parameter, while there is very insignificant displacement variation with respect to the third parameter.
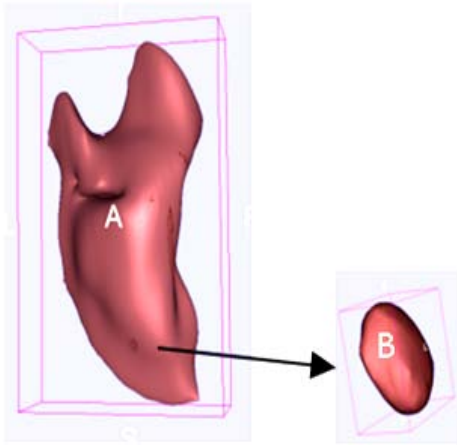
Figure 2.4: Surface of the lung (A) and tumor (B) after smoothing.
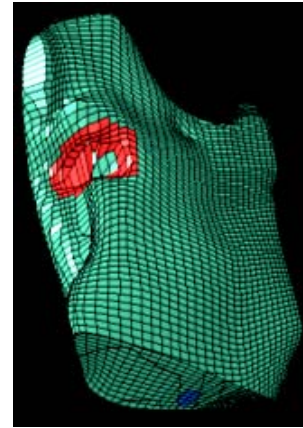
Figure 2.5: Finite element mesh of the lung. Red, blue and green show the trachea, tumor and parenchyma elements, respectively.
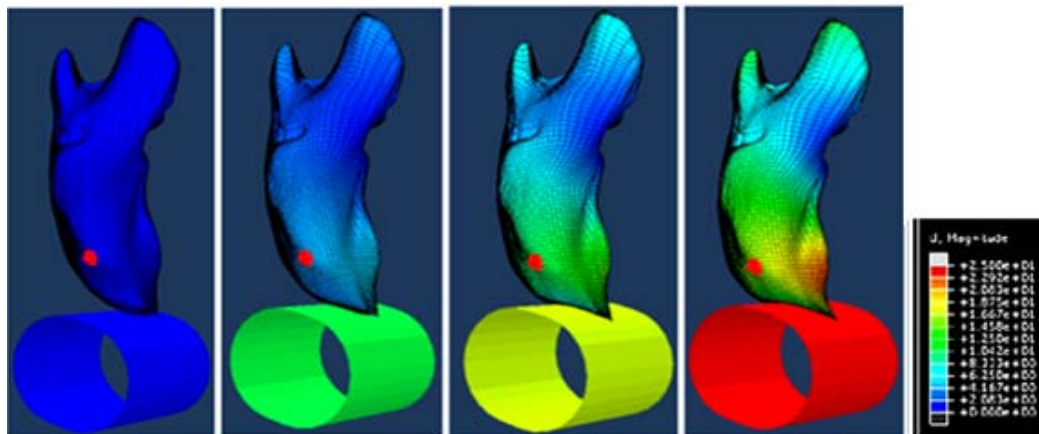
Figure 2.6: Four stages of the simulated respiration process. Far left: first stage without any deformation, far right: corresponds 25 mm contact body displacement and the two in the middle show intermediate stages. Red elements on the surface show marked surface near the tumor. Color bar on the right shows the displacements in mm.
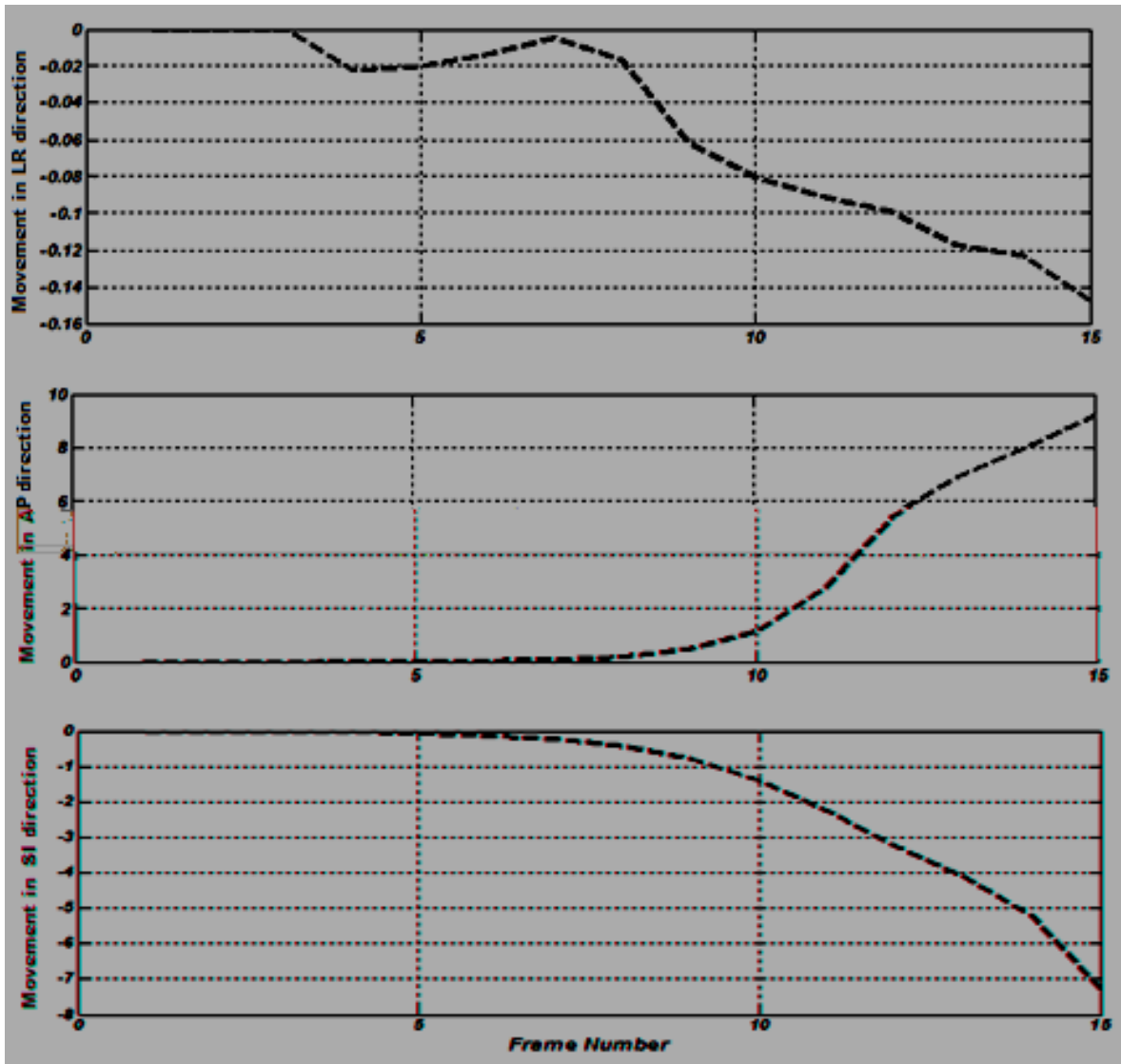
Figure 2.7: Mean displacement components of tumor nodes with respect to the cylindrical surface motion obtained from the finite element model. The model provides 15 motion frames where frame 15 corresponds to the 25mm cylinder displacement in the SI direction.

was used in this research, it needs significant amount of time to calculate the result. However, using an accelerated FE solver such as the one described in [17], tumor displacements can be determined intra-operatively as a function of the diaphragm's location which can be tracked using an electromagnetic motion tracking system in a real-time manner. The obtained results confirmed the ability of the method for tumor motion estimation. Moreover, to better simulate the diaphragm loading, the actual geometry of the diaphragm's contact surface must be incorporated. This can be obtained from in-vivo lung imaging and extracting the actual geometry of the diaphragm and use it as a contact problem. To have a better estimation of varying hyperelastic parameters, it is worth to conduct several experiments to measure them in different patients with different lung diseases and calculate the mean and standard deviations of each parameter. In this way, we will ensure about the robustness of the method to be applied clinically. This method will help the physicians to accurately implant the radioactive seeds within the cancerous tissue and consequently avoid under and/or over dosage. It leads to a successful treatment of lung cancer using brachytherapy similar to the brain and prostate cancer treatment by this method.

References

[1] A.W. Lin, A.L. Trejos, R.V. Patel, R. Malthaner, "Robot-assisted minimally invasive brachytherapy for lung cancer,"Telesurgery, Chap. 4, pp. 33-52 (2007).

[2] A.L. Trejos, A.W. Lin, M.P. Pytel, R.V. Patel, R.A. Malthaner, "Robot-assisted minimally invasive lung brachytherapy," International Journal of Medical Robotics and Computer Assisted Surgery 3, 41-51 (2007).

[3] V.W.K. Ng, J.E.S. Husband, V.M.C. Nicolson, I. Minty, A. Bamias, "CT evaluation of treatment response in advanced gastric cancer," Clin. Radiol. 51, 214-220 (1996).

[4] A.L. Trejos, R. Patel, R. Malthaner, "A device for robot-assisted minimally-invasive lung brachytherapy," presented at 2006 Conference on International Robotics and Automation, 15-19 May 2006.

[5] A.S. Naini, R.V. Patel, A. Samani, "A totally deflated lung's CT image construction by means of extrapolated deformable registration," presented at Progress in Biomedical Optics and Imaging, SPIEMedical Imaging, 10-16 Feb. 2011.

[6] N. Tselis, C. Kolotas, G. Birn, S. Röddiger, I. Filipowicz, M. Kontova, G. Fountzilas, P. Selviaridis, D. Baltas, R. Heyd, G. Anagnostopoulos, N. Zamboglou, "CT-guided interstitial HDR brachytherapy for recurrent glioblastoma multiforme: Long-term results," Strahlentherapie und Onkologie 183, 563-570 (2007).

[7] S. Nag, J.P. Ciezki, R. Cormack, S. Doggett, K. DeWyngaert, G.K. Edmundson, R.G. Stock, N.N. Stone, Y. Yu, M.J. Zelefsky, "Intraoperative planning and evaluation of permanent prostate brachytherapy: Report of the American Brachytherapy Society," International Journal of Radiation Oncology Biology Physics 51, 1422-1430 (2001).

[8] A. Al-Mayah, J. Moseley, K.K. Brock, "Contact surface and material nonlinearity modeling of human lungs," Phys. Med. Biol. 53, 305-317 (2008).

[9] A. Al-Mayah, J. Moseley, M. Velec, K. Brock, "Effect of friction and material compressibility on deformable modeling of human lung," Lect. Notes Comput. Sci. 5104 LNCS, 98-106 (2008).

[10] A. Al-Mayah, J. Moseley, M. Velec, K.K. Brock, "Sliding characteristic and material compressibility of human lung: Parametric study and verification," Med. Phys. 36, 4625-4633 (2009).

[11] Y.J. Zeng, D. Yager, Y.C. Fung, "Measurement of the mechanical properties of the human lung tissue," Transactions of the ASME. Journal of Biomechanical Engineering 109, 169-74 (1987).

[12] S. Pieper, M. Halle, R. Kikinis, "3D Slicer," presented at 2004 2nd IEEE International Symposium on Biomedical Imaging: Macro to Nano, 15-18 April 2004.

[13] A.S. Naini, R.V. Patel, A. Samani, "Measurement of lung hyperelastic properties using inverse Finite Element approach," IEEE Transactions on Biomedical Engineering 58, 2852-9 (2011).

[14] R. Werner, J. Ehrhardt, R. Schmidt, H. Handels, "Patient-specific finite element modeling of respiratory lung motion using 4D CT image data," Med. Phys. 36, 1500-1511 (2009).

[15] M. Urschler and H. Bischof, "Assessing breathing motion by shape matching of lung and diaphragm surfaces," presented at Physiology,Function,and Structure from Medical Images, SPIE Medical Imaging,13-15 Feb. 2005.

[16] S.C. Davies, A.L. Hill, R.B. Holmes, M. Halliwell, P.C. Jackson, "Ultrasound quantitation of respiratory organ motion in the upper abdomen," British Journal of Radiology 67, 1096-1102 (1994).

[17] R. Mousavi, I. Khalaji, A.S. Naini, K. Raahemifar, A. Samani, "Statistical finite element method for real-time tissue mechanics analysis," Comput. Methods Biomech. Biomed. Engin. 15, 595-608 (2012).

Chapter 3

Towards in-vivo Lung's Tissue Incompressibility Characterization for Tumor Motion Prediction during Lung Cancer Radiotherapy

(The Material presented in this chapter has been submitted to the Journal of Medical Physics as: Z. Shirzadi and A. Samani, "Towards in-vivo lung's tissue incompressibility characterization for tumor motion predication during lung cancer radiotherapy.")

3.1. Introduction

Although numerous efforts are ongoing for lung cancer treatment, recent statistics shows that lung cancer is the leading cause of cancer-related deaths in both men and women [1,2]. According to the American Cancer Society statistics in 2011, approximately 221,130 new cases of lung cancer were reported, accounting for 14% of cancer incidence. The same source reports that around 156,940 lung cancer-related deaths occurred in 2011, accounting for 27% of cancer-related deaths. Moreover, the 5-year survival rate for lung cancer is only 16%, which is very low compared to the 5-year survival rate of around 90% and 100% reported for breast cancer and prostate cancer, respectively [1]. Beside differences in the biological process of lung cancer compared to other types of cancer, low survival rate can be attributed to inadequate effectiveness of existing lung cancer treatment methods. Surgical resection which involves removing parts of the lung containing the tumor is one of the common current treatment methods [1,3,4]. However, lung cancer patients usually suffer from other lung diseases which result in poor

pulmonary system that could preclude choosing surgery as a viable treatment method [3,4]. Chemotherapy, another cancer treatment of choice, may lead to successful treatment outcome for patients in the early stages of lung cancer [1,3]. External beam radiation therapy, an alternative treatment technique, is commonly employed for lung cancer management at least as a complement treatment method [1,2,5]. Conventional radiotherapy treatment is performed in the clinic often based on a 3D image such as a 3D CT set obtained by averaging a 4D CT sequence [5,6]. Since the tumor is not static during the procedure, such single image is not sufficient for identifying the tumor's location throughout the procedure [5,7,8,9]. In fact, the major challenge in lung cancer treatment, particularly in methods where the tumor needs to be targeted (e.g. external beam radiation therapy and brachytherapy) is dealing with a moving target. What renders the problem even harder is that the motion amplitude in this context is large while its variation is less predictable. To compensate for tumor motion, a crude solution involves increasing the tissue volume to be irradiated such that the smallest tissue volume which encompasses the tumor during respiration is identified and irradiated throughout the procedure. This, however, would certainly lead to harmful radiation of healthy lung tissue while insufficiently irradiating the tumor volume [7,8,9]. In other words, with such method, normal tissue areas would undergo harmful radiation overdose while the tumor may receive insufficient radiation necessary to eradicate cancer cells. To reduce radiation overdosage and underdosage and meliorate the outcome of external beam radiation procedure, a dynamic targeted radiation technique whereby radiation beams are directed towards the moving tumor during respiration is highly desirable. The most critical prerequisite to develop such technique is determining tumor location throughout respiration [5,8,9]. For this purpose, imaging is not a viable option for beam radiation guidance as no imaging modality is currently available that can be employed effectively. While ultrasound imaging cannot be used because of lung air interference, CT imaging is associated with excessive amount of harmful ionizing energy and MR imaging is not suitable for lung real-time image guided applications.

As an alternative to the image guidance approach, computer-based modeling of the respiratory system mechanics can be utilized. In this approach, lung tissue deformation during respiration cycle can be estimated making it possible to determine tumor location

in real-time fashion. By developing a model that provides tumor location as a function of respiration cycle phase, a motion tracking system capable of determining the lung's respiration cycle phase can be utilized to find the tumor location over time during radiation. Different modeling approaches exist that can be adapted for this purpose. Among them, two major approaches have been considered which are based on:1) nonlinear image registration and 2) tissue biomechanics. In the image registration based techniques, the tumor motion estimation is obtained directly from 4D CT imaging data. Although several non-rigid image registration approaches were utilized to model motion fields in different studies [3,10,11,12,13], these techniques can be prone to errors associated with solution non-uniqueness and registration errors in some image regions especially where the gradient is low [5,14]. In general, registration based techniques are capable of motion field estimation for organs with small amount of deformation, whereas the respiratory system organ's deformation is large. The tissue biomechanics approach, on the other hand, benefits from the physical properties of soft tissue and respiration physiology [5,8,9] which can lead to higher accuracy, particularly to identify the internal structures motion including tumor motion. For attaining high level of realism, biomechanical models utilize image information for accurate delineation of the organ geometry and boundary conditions. In this approach, breathing dynamics and lung tissue deformation is modeled as a boundary value problem which can be solved numerically using finite element method (FEM) [5,15]. Apart from the biomechanical modeling which can be used in motion tracking by itself, the knowledge obtained from this model can be adapted for developing FEM based lung non-rigid image registration method similar to those described in [16,17].

Several studies have been conducted for biomechanical modeling of respiratory system since 1970. An early study modeled the lung as a cluster of nonlinear springs [8]. This was a seminal study that led to a large number of following research studies which modeled the lung utilizing springs. Afterwards, researchers proposed using FEM for biomechanical modeling of breathing dynamics. DeCarlo *et al* simulated the lung ventilation with FEM implementation of a 2D idealized lung. They considered the interaction between the lung and chest cavity by applying forces which expands the lung model during respiration [18]. A similar concept where 3D geometry idealization of the

lung was considered was utilized by Zhang *et al*, Villard *et al*, Eom *et al* and Werner *et al* [5,19,20,21]. In these studies, the respiration was modeled by applying negative pressure loading to the lung surface at the rest position while the lung expansion is restricted by the final volume of the lung or the chest cavity model. Werner *et al* [5] developed a mathematical lung phantom and lung cancer patient models for evaluation purposes. They used high resolution 4D CT image data of 12 lung cancer patients to analyze the accuracy of their proposed model. They examined different elasticity parameters (Young's modulus and Poisson's ratio) as well as various pressure forces to evaluate their influences on the phantom displacement field. They also assumed Young's modulus and Poisson's ratio values for the real patient models based on the phantom model and calculated the errors pertaining to different models. Al-Mayah *et al* performed a number of studies on lung ventilation mechanism simulation. The contact surface interaction between the chest wall and lung as well as material properties and homogeneity simplification were investigated in their studies. Throughout their modeling procedure, rather than pressure loading, displacement difference between inhale and exhale positions were applied as displacement boundary conditions to the lung model. They assessed their modeling precision using 16 lung cancer patient models with various tumor sizes and positions [8,9,14,22]. More recently, a lung biomechanical model developed specifically to estimate tumor motion in a deflated lung undergoing brachytherapy was described in [23].

Previous investigations which employed FEM to develop biomechanical models for respiration mechanism modeling have confirmed the feasibility and capability of FEM for respiration dynamics simulation. To achieve accurate biomechanical modeling of the respiring lung, and consequently, to estimate the location of the tumor with sufficient accuracy, we proposed a FE model capable of providing tumor trajectory information with respect to the respiration cycle phase. A prerequisite for utilizing this technique throughout a clinical procedure is to determine the diaphragm configuration in each phase of respiration which should be input to the proposed lung's biomechanical model as boundary condition. This information can be extracted from a limited number of fiducial markers that can be placed on the patient's chest and will be tracked using optical or electromagnetic tracking systems. Another prerequisite is 3D lung geometry which can

be obtained from the CT image acquired preoperatively for each patient. However, lack of accurate and reliable mechanical properties of lung tissue has been always a concern in the biomechanical modeling process. As mentioned earlier, a number of studies were conducted to measure these parameters or to evaluate the impact of mechanical parameters variation on the model accuracy [5,8,9,20,24]. Nevertheless, accurate characterization of a very important parameter has been overlooked in studies conducted to-date. Since the amount of air within the lung issue is known to vary significantly during respiration, it is reasonable to expect that the tissue mechanical properties also change significantly during respiration. To model these variations one approach is idealizing the lung tissue as a biphasic material consisting of soft tissue and variable air phases. Such approach is quite involved both in terms of computations and constitutive relation parameters measurement; hence a simpler and more practical alternate approach is desirable. In this study, we propose such an alternate approach where we assume that the lung tissue is elastic or hyperelastic material with incompressibility that varies throughout respiration in response to air volume variation within the tissue. To accomplish reliable biomechanical modeling of the respiratory system, a parameter characterizing tissue incompressibility is required. As such, this investigation is dedicated for estimating incompressibility parameter variation of the lung tissue and representing this variation as a function of respiration cycle time. First, we conducted a numerical phantom study to demonstrate the significance of using varying incompressibility parameter over a constant incompressibility parameter throughout respiration cycle. This phantom study demonstrated that considering varying incompressibility is critical to achieve accurate tumor motion characteristics. The proposed tissue incompressibility characterization technique is formulated using an optimization algorithm where incompressibility parameters are sought that lead to the best similarity between acquired 4D CT images of the lung and corresponding images obtained using the lung's biomechanical model. To assess the performance of the proposed technique, a porcine animal model was used. In this model, we sought to calculate the porcine lung incompressibility parameter as a function of the respiration cycle phase. To assess the advantage of using variable incompressibility parameter over constant parameter in this animal model, we utilized the technique to calculate a constant incompressibility

parameter throughout respiration. Comparison of images obtained from these two biomechanical models with their corresponding acquired CT images demonstrated that considering variable incompressibility parameter leads to significantly better model.

3.2. Methods and Materials

To characterize lung tissue incompressibility, we use Poisson's ratio in conjunction with linear elastic or Marlow hyperelastic models [8]. For modeling incompressibility variation resulting from air content variation within the tissue during respiration, we obtain discrete variable values of the Poisson's ratio in different times over the course of respiration cycle. Given that respired air inside the lung is not fully constrained within the tissue i.e. the air can flow out of the alveoli as a result of tissue compression, it is reasonable to expect that the Poisson's ratio decreases during inspiration while it increases during expiration. This implies that the lung tissue Poisson's ratio and lung volume vary in opposite directions during respiration. A typical lung volume variation over a respiration cycle is shown in Figure 3.1 [25,26,30]. This figure shows significant lung volume variation during respiration which stems from changing the amount of inhaled air. A variation in the opposite direction is expected to exist for the lung tissue Poisson's ratio.
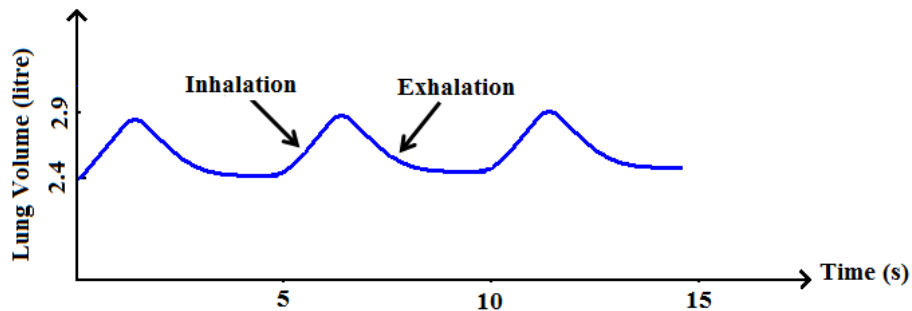
Figure 3.1: Lung volume variation throughout inhalation and exhalation phases with typical 12 breaths per minute. A variation in the opposite direction is expected to exist for the lung tissue Poisson's ratio.

3.2.1. Numerical phantom study

In order to investigate the influence of using variable incompressibility parameter on tumor movement estimation throughout respiration, we first conducted a numerical phantom study. In this study, a FE model of a lung phantom was constructed before it was subjected to simulated negative pressure load to mimic lung deformation during inspiration. The purpose here is to assess the impact of following the conventional incompressibility idealization of having a constant Poisson's ratio instead of a more realistic approach of using variable Poisson's ratio on lung tumor motion during respiration. Significant difference between tumor motions obtained by these two approaches would imply that considering variable incompressibility parameter is necessary for predicting reliable tumor motion. In this study, a cylindrical phantom model with 2 liters volume, which is similar to a normal human lung volume at the end of expiration, was developed to initiate the first phase of respiration simulation [5,25]. A FE mesh with 22896 eight-noded hexahedral elements was generated for this phantom. A rigid cylindrical surface including a circular surface at the top end was also considered in the model to mimic the chest cavity. The size of this cylinder was designed such that its internal surface has a gap with the phantom's surface. This gap is gradually filled after applying negative pressure. The volume of space inside this cylinder is 3 liters which is consistent with a typical human chest cavity [5,25]. In this study, the inspiration phase was used to characterize tissue incompressibility. For this purpose, a frictionless contact mechanics model was used to simulate the interaction between the lung phantom and the cylindrical surface during inspiration. A number of lung surface nodes that model the trachea's interface with the lung were fixed to provide the FE model's zero-displacement boundary conditions [5,9,20,23,27]. To model the diaphragm muscle, a cluster of springs uniformly spread over the bottom circular surface of the lung phantom were utilized. These springs become active during the expiration phase only. To calculate the springs' constants, we assumed that the phantom's circular diaphragm works in bending mode. Accordingly, bending stiffness distribution of a clamped circular plate was estimated based on a thickness of 3.5 mm and a Young's modulus of 100 kPa, which are both reported in the literature for the diaphragm muscle [13,27,28]. Based on this estimation, we obtained an average spring constant value of 171.6 N/m per each unit area of 1 mm^2.

In the phantom, the tumor to be tracked was considered spherical with a Young's modulus and Poisson's ratio values set to 18 kPa and 0.49, respectively. Figure 3.2 demonstrates the FE model of the lung phantom including the tumor along with the rigid cylindrical surface of the chest cavity and the diaphragm mimicking springs.
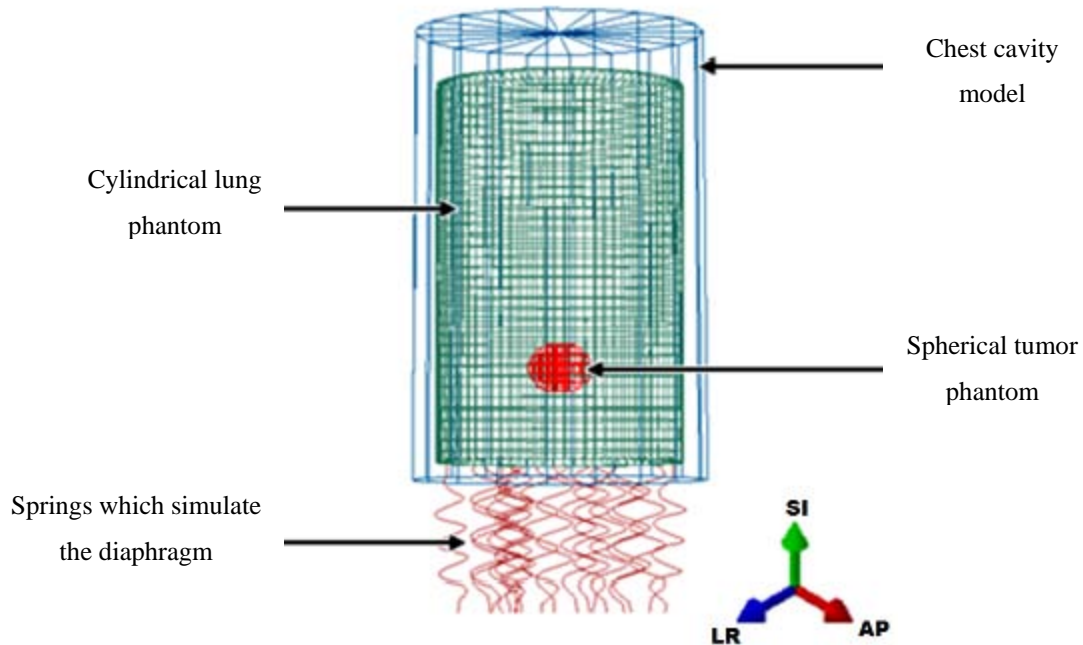
Figure 3.2: The phantom model utilized to investigate the effect of time variable Poisson's ratio. The model components including cylindrical lung tissue mimicking phantom (green color), closed rigid cylinder mimicking the chest cavity (blue color) and springs (red color) which mimic the diaphragm are shown.

To investigate the influence of using varying incompressibility parameter over constant incompressibility parameter, we conducted three simulations. In the first simulation, the lung tissue was considered as linear elastic model with a constant Poisson's ratio which is the simplest model used by some investigators [5,8,9,20,27]. In the second simulation, a Marlow hyperelastic model with a constant Poisson's ratio was used in the FE model. This model presents a better approximation compared to the first one as it takes into account tissue nonlinearity. It is similar to traditional models used by a number of investigators [9,22]. In the third simulation, a Marlow hyperelastic model with variable Poisson's ratio was considered. Although, the amount of required pressure loading is

unknown for lung biomechanical modeling [5], pressure variation during respiration is reported in the literature [25,29]. In this simulation, variable pressure loading function of time which exhibits pressure variations similar to the reported variations was applied to the phantom's surface throughout inspiration. Compared to the first and second biomechanical models, this model is expected to be the most realistic one as it accounts for tissue nonlinearity, variable incompressibility and pressure variations. Hence, its results will be considered as the testground truth. In the constant incompressibility simulations, a pressure equal to the final amount of the applied pressure function was considered. Moreover, a Poisson's ratio equal to the mean value of Poisson's ratios applied in the third simulation was taken into account in the two cases with constant Poisson's ratio. FEM was used to determine the tumor's motion for each case while geometric nonlinearity was taken into account for all the simulations and both geometric and intrinsic nonlinearities were considered for the latter two simulations.

3.2.2. Optimization algorithm for the Poisson's ratio calculation

To determine discrete variable values of the lung tissue's Poisson's ratio, we developed an optimization algorithm. A block diagram of this algorithm is shown in Figure 3.3. The essence of this algorithm is to find a Poisson's ratio corresponding to each given time point such that it results in the maximum similarity between the lung's acquired and simulated CT images. The simulated images are constructed using the lung's acquired end exhale CT image combined with tissue displacements obtained from the lung's FE model at each time point. In the lung's FE model, the respiration loading is idealized as unknown variable negative pressure applied to its surface [5]. As such, to obtain the sought Poisson's ratio, it is changed systematically along with the pressure loading in each respiration time point until the maximum similarity between corresponding acquired and simulated images is achieved. To achieve this purpose, a combined cost function was used which takes into account the lung image volumetric information and its segmented surface. This function was formed based on image and surface Sum Squared Differences (SSD) which is known to be a suitable similarity measure for single modality images [30]. As such, the following optimization problem was formulated:

$$\text{Minimize } F(v, p) = SSD_I + \omega \, SSD_S$$
$$\text{sub. to } 0.2 \leq v \leq 0.45 \text{ and} - 50 \, kPa \leq p \leq 0$$

where v and p are the Poisson's ratio and pressure value to be determined by the optimization algorithm. SSD_I is the sum squared differences between the acquired and simulated lung images while SSD_S is the sum squared differences between the lung's surfaces obtained by segmenting the acquired and simulated images. The weight factor ω was considered to allow variable weight necessary to emphasize volumetric or surface image information. Our analysis indicated that $\omega = 10$ is a proper choice. The optimization method that was utilized to solve this multi-variable optimization problem is a variant of the Nelder-Mead method which, unlike the original method, can solve constrained optimization problems [31]. In addition to the variables lower and upper bounds, this method requires calculating the objective function value corresponding to the updated variables estimate while it does not require calculating the function's derivatives. This optimization algorithm starts with an initial guess of the Poisson's ratio (v) and the pressure parameter (p), and it varies them systematically until optimal values corresponding to the minimum objective function are obtained. After finding the optimum values of the Poisson's ratio and pressure in each inhalation time point staring from end exhalation, we fitted a number of functions to the values to achieve the best match functions which were second order polynomial for the obtained Poisson's ratios and third order polynomial function for the pressure values.
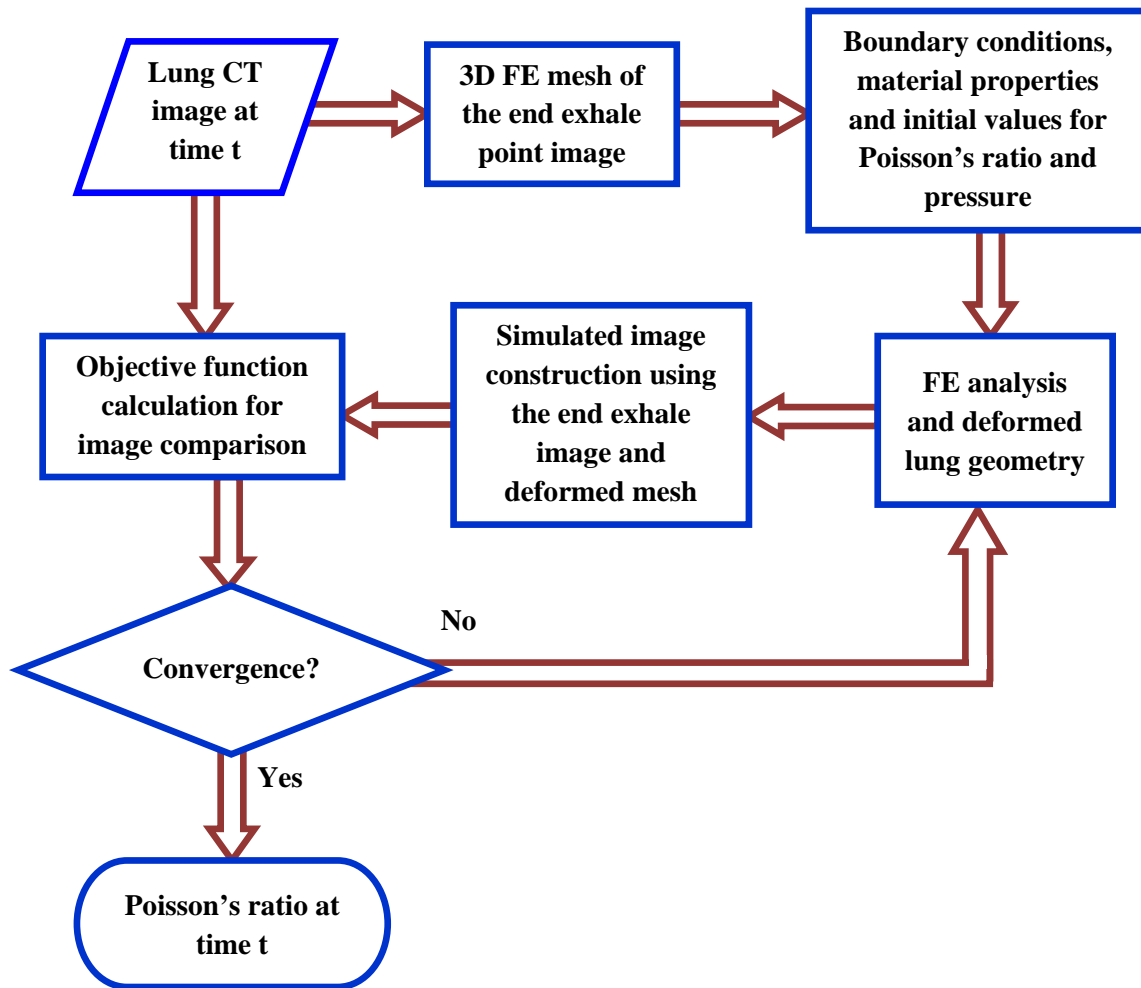
Figure 3.3: Optimization algorithm block diagram developed for the lung tissue variable Poisson's ratio measurement.

To calculate the objective function value corresponding to a current set of v and p variables, the lung CT image corresponding to the end exhale point is used as the undeformed lung image. Using this image, we construct the lung's 3D FE model with the current v value and load it incrementally with the current pressure value of p in order to obtain the lung's model nodal displacements in each respiration point. To construct the lung's simulated images, we warp the undeformed lung CT image using Thin Plate Spline (TPS) technique in which nodal displacements obtained from the FE analysis corresponding to each given time point during the inhale phase were considered as

warping landmarks' displacements. Details of the lung's FE mesh construction and modeling are given later in the Methods section.

3.2.3. Ex-vivo porcine lung model

3.2.3.1. 4D CT imaging and 3D model construction

As mentioned earlier, to examine the feasibility of the proposed technique to determine a time variable lung tissue incompressibility parameter during the respiration cycle, 4D CT image sequence of the lung's respiration dynamics is required. To obtain the 4D CT images, we conducted an experiment involving an ex-vivo porcine lung. In this experiment, the lung was respired using a mechanical ventilator with 12 breath/minute respiration frequency. The images were acquired using GE Healthcare Discovery CT 750 HD scanner. The CT scanning parameters were set to 80 kVp, 200mA and a gantry rotation period of 0.4 sec. To acquire the region of interest in the images, background parts of the original scans were cropped; therefore, the 4D CT image sequence we employed in this investigation had a final image size of $(512 \times 260 \times 308)$ voxels with a voxel size of $(0.43 \times 0.43 \times 1.25)$ mm^3 [32]. Figure 3.4 shows one slice of the 4D CT image data set in the sagittal view in different respiration phases. To generate 3D lung's FE model, we first constructed the 3D volume of the lung tissue. To accomplish this, the lung tissue was segmented from other parts of the image in each 2D slice of the end exhale image using 3D Slicer software package [33]. Next, these segmented slices were input into the slicer model maker module to construct a 3D model. The 3D model construction was followed by surface smoothing with a Laplacian filter to remove the sharp artifacts caused by model construction filter and segmentation process.
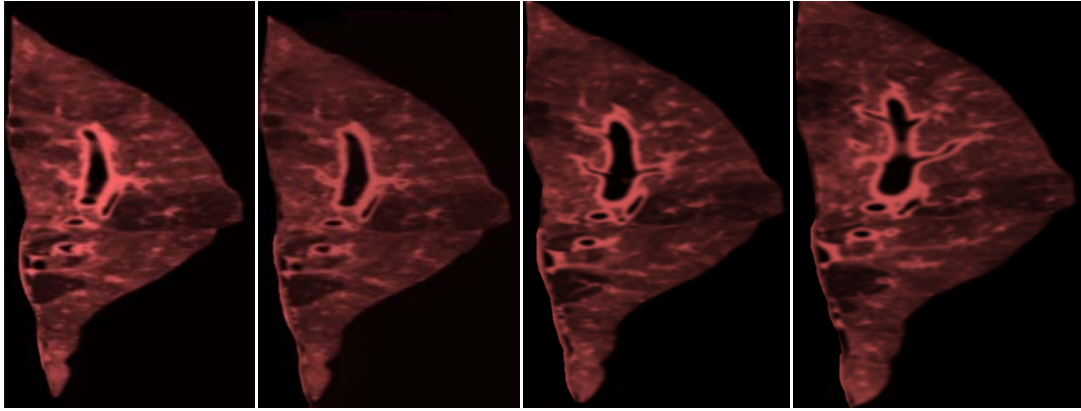
Figure 3.4: 2D slices of the ex-vivo porcine lung 4D CT image sequence. Left to right: end exhale to end inhale lung images.

3.2.3.2. Lung FE model

The acquired 3D lung image volume in the end exhale phase was used to generate a FE mesh with 22350 eight-noded hexahedral elements and 25610 nodes by employing IA-FEmesh open source software [33]. After FE mesh generation, tissue mechanical parameters were input while loading and boundary conditions were applied in each iteration. For the lung tissue mechanical properties, we considered a Young's modulus value of 1.15 kPa for the linear elastic model while we used data obtained from our previous studies on porcine lung [24] in conjunction with the Marlow hyperelastic model. The Young's modulus in the linear elastic case represents the tangent of the approximately linear portion of the hyperelastic tissue's stress-strain curve [9,24]. To investigate the influence of using variable incompressibility with the hyperelastic model, two cases of constant and variable Poisson's ratio were considered. However, to be able to assess the impact of using hyperelastic model and linear elastic model with variable incompressibility, for the linear elastic analysis only one case of variable Poisson's ratio was considered.

For in-vivo lung FE analysis, proper modeling of the interaction between the lung and chest cavity is critical to achieve desirable accuracy. This interaction can be simulated using a contact mechanics FE model while nodes representing the interface between the trachea and lung's surface are fixed in all three directions to provide the model's zero

displacements boundary conditions [5,9]. For loading the lung's model, pressure was applied to its surface. For in-vivo applications, the intrapleural pressure is generated inside the chest cavity as a result of the chest volume variation and it is less than the atmospheric pressure during respiration. The other respiratory system pressure is the intrapulmonary pressure which is smaller than atmospheric pressure during inspiration and higher than it throughout expiration. As stated earlier, the amount of the equivalent pressure for tissue biomechanical modeling is unknown; hence it was treated as a variable to be determined through the optimization algorithm. This pressure was shown to be highly dependent on the material properties of the lung tissue [5]. In the present study where ex-vivo lung was tested, the boundary conditions are different from those of in-vivo case. Throughout the 4D CT image acquisition process, the lung tissue was placed on the scanner table. The acquired 4D CT images indicated that the contact surface between the lung and scanner table varied very slightly throughout the lung inflation (inhale) process. As such, we considered fixed boundary conditions at the set of nodal points of this surface area. Moreover, nodal points of the lung tissue where the trachea was attached were also fixed. To obtain simulated inhaled lung images, we considered four time points for breathing from end exhale to end inhale. After constructing the undeformed lung's FE mesh corresponding to the end exhale phase image, FE analysis was conducted using current estimates of pressure and Poisson's ratio utilizing ABAQUS software (DassaultSystčmesSimulia Corp., Providenec, RI, USA). Figure 3.5 shows the resultant FE model of the lung and its boundary conditions as well as the deformed FE mesh. An image based on this analysis was constructed using MATITK software [34]. The image construction was performed using RegisterThinPlateSpline (rtps) warping method [35] in which the FE nodal displacements were used as landmarks. As indicated earlier, the iterative constrained Nelder-Mead method [31] was employed in conjunction with the lung's FE model and image warping module to calculate the objective function value in each iteration. To ensure optimization solution uniqueness, several initial guess values of the pressure and Poisson's ratio as well as lower and upper bounds were considered in each respiration time point.
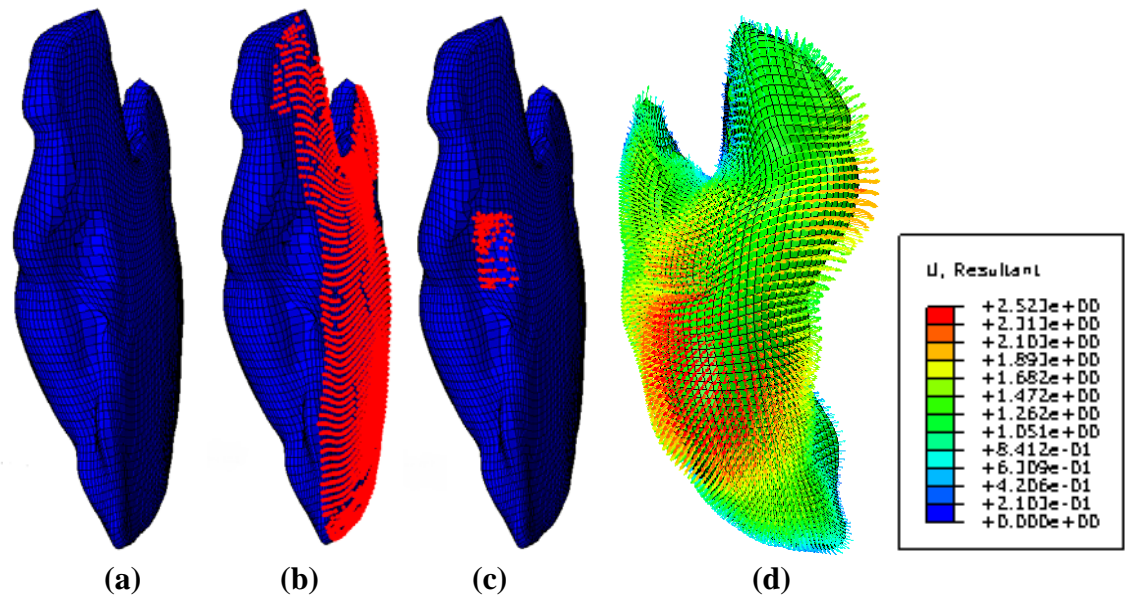
Figure 3.5: a) 3D FE mesh of the porcine lung in the end exhale phase, b) red points represent nodes related to part of the lung that does not move throughout ventilation, c) trachea related nodes which are assumed to be fixed during respiration and d) the resultant displacement field obtained by applying pressure loading in one phase of ventilation; the color bar shows the displacements in cm.

3.2.3.3. Validation

In order to validate the Poisson's ratio results obtained from the inhale phase, we utilized the porcine lung images acquired during the expiration phase of ventilation. Thus, we constructed a FE model with the same boundary conditions from the lung's end inhale image. For modeling the expiration phase, similar to the inspiration phase, four increments were considered to simulate which FE analysis was conducted using both linear elastic and Marlow hyperelastic material properties similar to the inspiration phase simulations. Assuming that expiration is similar to inhalation with a reversed time order, we used the $v(t)$ and $p(t)$ functions calculated for the inspiration phase to calculate $v(T_{inhale} - t)$ and $-p(T_{inhale} - t)$ as the Poisson's ratio and pressure functions over the expiration phase. Here, T_{inhale} is the end inspiration time and the minus sign is used since the applied pressure is positive through the expiration simulations. These functions were applied in each expiration time point FE simulation and similar to the inspiration phase

simulation, a lung image corresponding to each expiration time point was constructed. The same analysis was also conducted for the Marlow hyperelastic case with constant Poisson's ratio. The pressure function ($-p(\mathrm{T_{inhale}} - \mathrm{t})$) and Poisson's ratio ($v$) calculated based on inspiration phase were applied to the FE mesh of the end inhale image and images corresponding to all expiration time points were constructed. Accuracy of the obtained Poisson's ratio functions calculated from elastic and hyperelastic analysis and the constant Poisson's ratio were assessed by comparing difference images obtained from the reconstructed images and their acquired CT image counterparts over the expiration phase.

3.3. Results

3.3.1. Numerical lung phantom study

To assess the impact of using variable tissue Poisson's ratio, as was indicated in the Methods section, the lung phantom was analyzed in two cases of variable Poisson's ratio and constant Poisson's ratio. Under each one of these cases, the lung tissue was assumed to be hyperelestic obeying Marlow model. To compare the results, the case with constant Poisson's ratio was also analyzed for linear elastic lung tissue. The case involving variable Poisson's ratio in conjunction with Marlow model was considered as the "testground truth". Figure 3.6.a and 3.6.b show the input pressure and Poisson's ratio functions, respectively, which were considered in the time variable incompressibility case. Since inhalation phase is modeled in this study, 2 sec. duration was considered for FE modeling. For the constant incompressibility cases, the Poisson's ratio mean value was taken into account. Figure 3.6.cillustrates the tumor's trajectory main component in the SI direction obtained by the linear elastic model and the Marlow hyperelastic models without and with variable incompressibility. The latter two hyperelastic models are labeled Marlow 1 and Marlow 2. The final tumor displacement components in the linear elastic case and the Marlow hyperelastic cases are summarized in Table 3.1. The information extracted from Table 3.1 and Figure 3.6.cdemonstratesignificant differences between tumor motions obtained using the constant and time variable Poisson's ratio models. Moreover, in each simulation case, tumor displacements in the LR and AP directions are similar since the spherical tumor's position is symmetric with respect to the

LR and AP axes. Comparison between results obtained from the linear elastic and Marlow hyperelastic models with constant Poisson's ratio indicates that incrementally more realistic modeling that considers hyperelastisity has a substantial impact on the tumor motion estimation. To isolates the impact of incompressibility variation results obtained from the hyperelastic models with constant and variable Poisson's ratio were compared. In this comparison, Table 3.1 indicates that the tested ground truth tumor motion amplitude is more than three times larger than the amplitude obtained from Marlow model with constant incompressibility. This demonstrates that ignoring tissue incompressibility variation accounts for a substantial amount of displacement deviation from its ground truth counterpart.

(a)

(b)

(c)
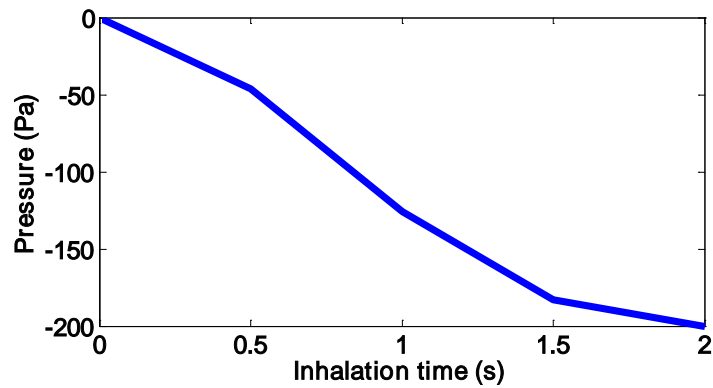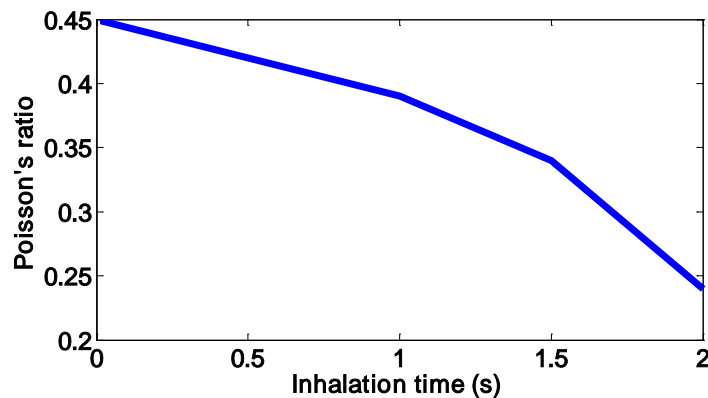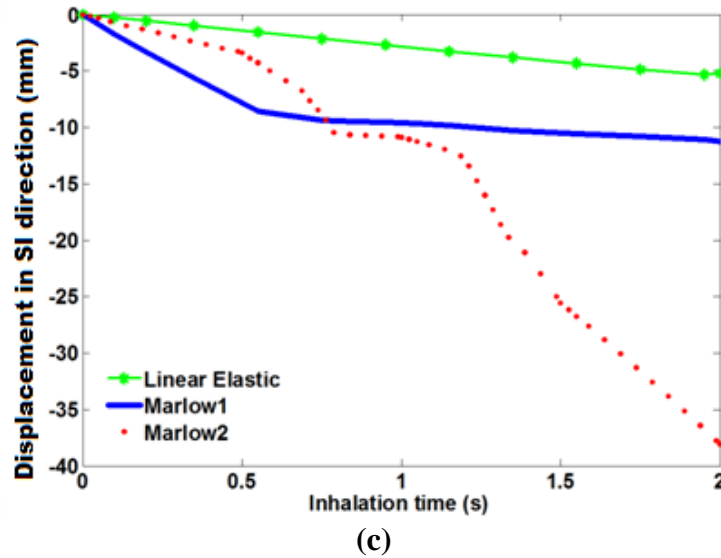
Figure 3.6: a) and b) Pressure and Poisson's ratio functions of inhalation time applied to the phantom lung tissue, respectively. c) Tumor trajectory components in the SI direction obtained from linear elastic material model with constant Poisson's ratio, Marlow hyperelastic model with constant Poisson's ratio (Marlow1), and Marlow hyperelastic model with time variable Poisson's ratio (Marlow2).

Table 3.1: Tumor movement results obtained from the linear elastic and Marlow hyperelastic analysis. All the displacement numbers are in mm.

Material Properties	Tumor Displacement in LR Direction	Tumor Displacement in AP Direction	Tumor Displacement in SI Direction	Total Tumor Movement
Elastic with constant incompressibility	3.18	3.02	-5.19	6.80
Hyperelastic with constant incompressibility	2.78	2.70	-11.23	11.88
Hyperelastic with variable incompressibility	-0.04	-0.16	-38.10	38.10

3.3.2. Incompressibility function of cyclic time for an ex-vivo porcine model

As described in the Methods, the lung tissue's Poisson's ratio function of an ex-vivo porcine model was determined using linear elastic model and a Marlow hyperelastic model. Four time increments were considered to cover the inhale phase while the Poisson's ratio and pressure were assumed to be constant over each increment. In order to compare the proposed hyperelastic model with variable Poisson's ratio with the more conventional hyperelastic model with a constant Poisson's ratio, a Marlow hyperelastic model with constant Poisson's ratio was also analyzed. In this analysis, the Poisson's ratio was assumed to be constant while the pressure was set to vary incrementally. In the optimization process used for determining variable incompressibility, the Poisson's ratio was constrained between 0.2 and 0.45 [5] while the pressure was allowed to vary between -50 kPa and 0 [29]. After running the optimization algorithm for each increment, the Poisson's ratio and pressure values as well as the amounts of cost function for each increment corresponding to the linear elastic model were obtained and summarized in Table 3.2. Also, the pressure, Poisson's ratio and cost function values obtained from the hyperelastic model with variable Poisson's ratio are given in Table 3.3. Results summarized in Tables 3.2 and 3.3 indicate that using linear elastic or hyperelastic model does not have a significant impact on the calculated Poisson's ratio values while the pressure values obtained from these two models are substantially different. This implies that the pressure is more sensitive to the tissue stiffness model and extra care needs to be taken in selecting a more realistic tissue stiffness model in order to obtain a reliable pressure function if necessary. To obtain functions that describe their time variability, the obtained Poisson's ratio and pressure values, were fitted using a quadratic and third order polynomial functions, respectively. The fitting curves are shown in Figure 3.7 and Figure 3.8 for the linear elastic and Marlow hyperelastic models, respectively. The pressure curves exhibit variation trends that are consistent with those reported in the literature [25,29].

The obtained pressure and Poisson's ratio functions for the linear elastic case are:

$$v = -0.0312t^2 - 0.0021t + 0.4143$$

$$p = 11.7933t^3 - 27.6057t^2 - 19.1469t + 0.0641$$

and for the Marlow hyperelastic model, they are:

$$v = -0.0199t^2 - 0.0356t + 0.4257$$

$$p = 2.06t^3 - 4.6t^2 - 3.725t + 0.023$$

where v and p are the Poisson's ratio and pressure, and t represents the inhalation phase time. Note that these functions are obtained based on data corresponding to the inhalation phase of respiration only; as such their validity is limited to this phase.

Table 3.2: Incremental pressure and Poisson's ratio values obtained from the optimization technique with the linear elastic model in addition to corresponding values of SSD_I , SSD_S and the cost function. These are the optimum values obtained using several initial guesses and lower and upper bounds.

Phase Number	Pressure (kPa)	Poisson's ratio	SSD_I	SSD_S	Cost function
1 (0-0.5 s)	-14.68	0.4061	543.72	62.72	1171
2 (0.5-1 s)	-35.28	0.3790	1100.5	93.70	2037.5
3 (1-1.5 s)	-50.71	0.3429	836.74	53.06	1367.4
4 (1.5-2 s)	-54.37	0.2846	315.74	33.46	650.4

Table 3.3: Incremental pressure and Poisson's ratio values obtained from the optimization technique with the Marlow hyperelastic model in conjunction with variable Poisson's ratio in addition to corresponding values of SSD_I , SSD_S and cost function. These are the optimum values obtained using several initial guesses and lower and upper bounds.

Phase Number	Pressure (kPa)	Poisson's ratio	SSD_I	SSD_S	Cost function
1 (0-0.5 s)	-2.64	0.4053	544.14	62.74	1171.6
2 (0.5-1 s)	-6.38	0.3631	1221.4	85.6	2077.5
3 (1-1.5 s)	-8.87	0.3347	840.48	51.94	1360
4 (1.5-2 s)	-9.37	0.2726	333.55	33.15	665.06

(a)   (b)
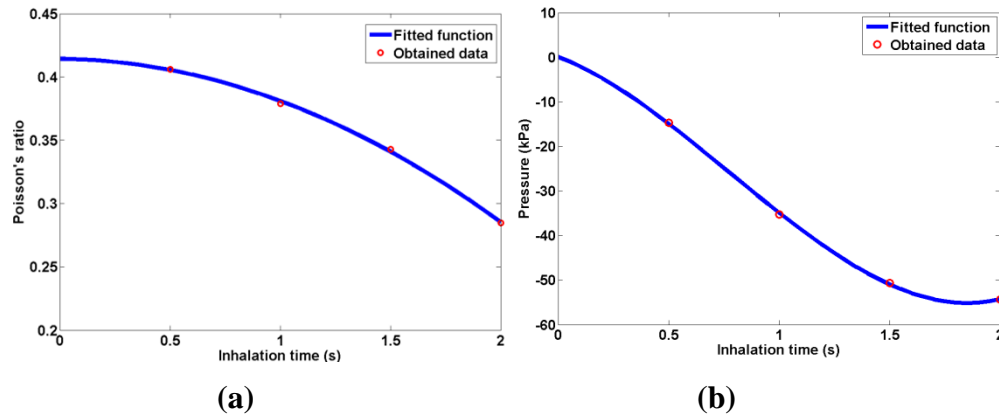
Figure 3.7: a) Poisson's ratio and b) Pressure functions of the inhalation phase corresponding to the linear elastic model. The red Points represent data obtained from the optimization technique.
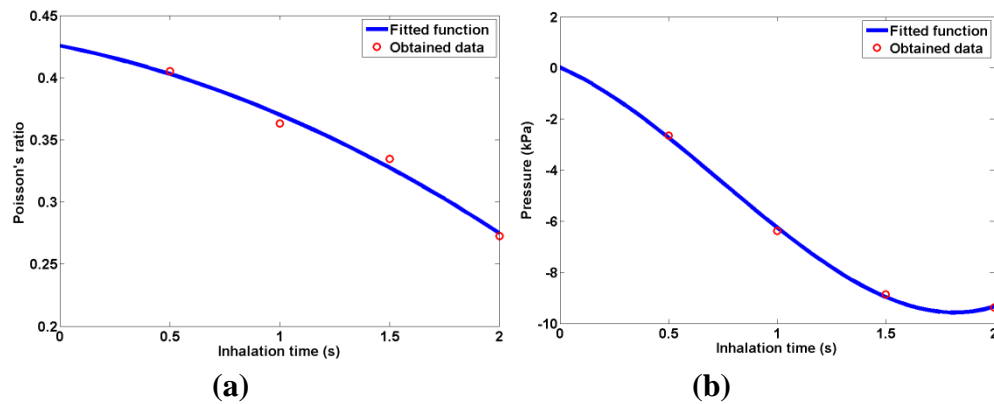
Figure 3.8: a) Poisson's ratio and b) Pressure functions of the inhalation phase corresponding to the Marlow hyperelastic with variable Poisson' ratio model. The red Points represent data obtained from the optimization technique.

Results obtained from the Marlow model in conjunction with constant Poisson's ratio are summarized in Table 3.4. This table shows almost an order of magnitude increase in the cost functions compared to values obtained with variable Poisson's ratio. This provides a strong hint that using variable Poisson's ratio over a constant Poisson's ratio constitutes more realistic tissue idealization evident by much more acquired and simulated image similarity.

Table 3.4: Incremental pressure and Poisson's ratio values obtained from the optimization technique with the Marlow hyperelastic model in conjunction with a constant Poisson's ratio in addition to the corresponding values of SSD_I , SSD_S and cost functions. These are the optimum values that were obtained using several initial guesses and lower and upper bounds.

Phase Number	Pressure (kPa)	Poisson's ratio	SSD_I	SSD_S	Cost function
1 (0-0.5 s)	-1.52	0.2956	619.2	58.25	1201.7
2 (0.5-1 s)	-3.49	0.2956	2094.7	145.6	3550.7
3 (1-1.5 s)	-5	0.2956	3198.6	194.6	5144.6
4 (1.5-2 s)	-5.22	0.2956	3557.5	218.86	5746.1

The SSD_I values reported in the tables show similarity of the volumetric image information while the SSD_S values indicate similarity of the images segmented surfaces. The former actually provides a measure for volumetric anatomical consistency between acquired and simulated images. The significantly smaller SSD_I values given in Tables 3.2 and 3.3 signify improved volumetric anatomical consistency obtained with the variable Poisson's ratio model compared to that of the constant Poisson's ratio model. This implies that tissue idealization that takes into account variable tissue incompressibility is highly important for precise tumor location prediction during respiration.

3.3.3. Ex-vivo porcine model results validation

As described in the Methods section, the pressure and Poisson's ratio values obtained using the inhalation image information were properly used as input in the corresponding exhalation time points. Using these input values corresponding simulated lung images were obtained and compared to their experimental counterparts. Results obtained in this part are summarized in Table 3.5, Table 3.6 and Table 3.7 corresponding to the linear elastic model and the Marlow hyperelastic models in conjunction with variable and constant Poisson's ratio.

Table 3.5: Incremental SSD_I , SSD_S and cost function values obtained from the validation process over the exhalation phase with the linear elastic model with the pressure and variable Poisson's ratio obtained from the inhalation phase analysis.

Phase Number	Pressure (kPa)	Poisson's ratio	SSD_I	SSD_S	Cost function
1 (0-0.5 s)	3.66	0.2846	452.6	53.18	984.4
2 (0.5-1 s)	19.09	0.3429	1677.4	52.57	2203.1
3 (1-1.5 s)	39.69	0.3790	1633.8	56.44	2198.2
4 (1.5-2 s)	54.37	0.4061	829.8	43.51	1265

Table 3.6: Incremental SSD$_I$, SSD$_S$ and cost function values obtained from the validation process over the exhalation phase with the Marlow hyperelastic model with the variable Poisson's ratio and pressure values obtained from the inhalation phase analysis.

Phase Number	Pressure (kPa)	Poisson's ratio	SSD$_I$	SSD$_S$	Cost function
1 (0-0.5 s)	0.5	0.2726	452.6	53.18	984.4
2 (0.5-1 s)	2.99	0.3347	1709.5	57.82	2287.7
3 (1-1.5 s)	6.73	0.3631	1530.4	67.95	2209.9
4 (1.5-2 s)	9.37	0.4053	768.82	43.46	1203.4

Table 3.7: Incremental SSD$_I$, SSD$_S$ and cost function values obtained from the validation process over the exhalation phase with the Marlow hyperelastic model with the constant Poisson's ratio and pressure values obtained from the inhalation phase analysis.

Phase Number	Pressure (kPa)	Poisson's ratio	SSD$_I$	SSD$_S$	Cost function
1 (0-0.5 s)	0.22	0.2956	550.7	65.43	1205.1
2 (0.5-1 s)	1.73	0.2956	1386.8	87.55	2262.3
3 (1-1.5 s)	3.7	0.2956	3200.8	111.7	4317.8
4 (1.5-2 s)	5.22	0.2956	3099.1	271.87	5817.8

For comparison and further assessment of the performance of each material model, 2D slices of the difference images between constructed images and their corresponding 4D CT counterpart are calculated at four time points during inhalation and shown in Figure 3.9, Figure3.10 and Figure3.11 for the linear elastic and the two Marlow hyperelastic models, respectively. Figures 3.9 and 3.10 provide visual qualitative confirmation of the reliability of the calculated Poisson's ratio and pressure functions for the exhalation phase as there is little image information in the shown difference images. Figure 3.11, which

corresponds to the Marlow model in conjunction with constant Poisson's ratio, shows significantly more image information compared to both of the linear elastic and hyperelastic models with variable Poisson's ratio. Tables 3.5, 3.6 and 3.7 provide valuable information for quantitative assessment. Tables 3.5 and 3.6 indicate that the cost function values obtained from the linear elastic and hyperelastic model with variable Poisson's ratio are small and similar to their inhalation phase counterparts. Cost function values given in Table 3.7 are also similar to corresponding values given in Table 3.4. These values are significantly larger than those obtained with using variable Poisson's ratio based models. This again highlights the superiority of using variable incompressibility over constant incompressibility parameter.
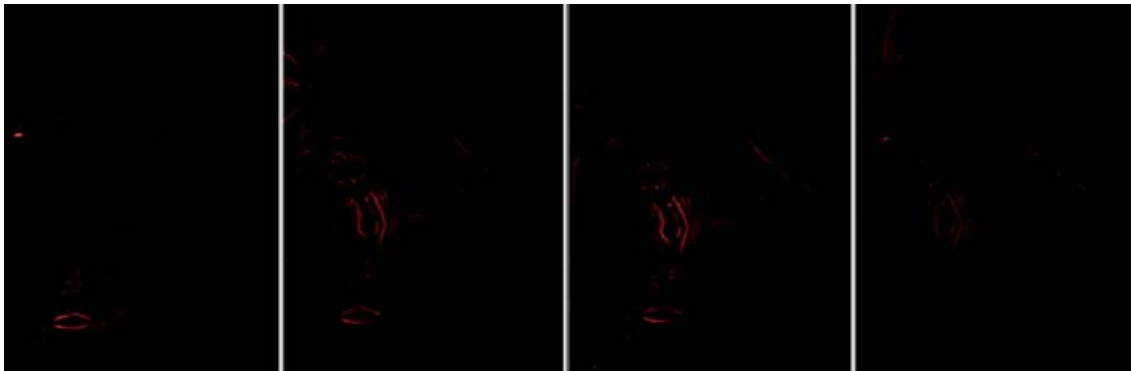
Figure 3.9: Difference images between 2D slices of the 4D CT image acquired during exhalation and its corresponding image simulated using the linear elastic model with variable Poisson's ratio. Left to right correspond to end inhale to end exhale images.
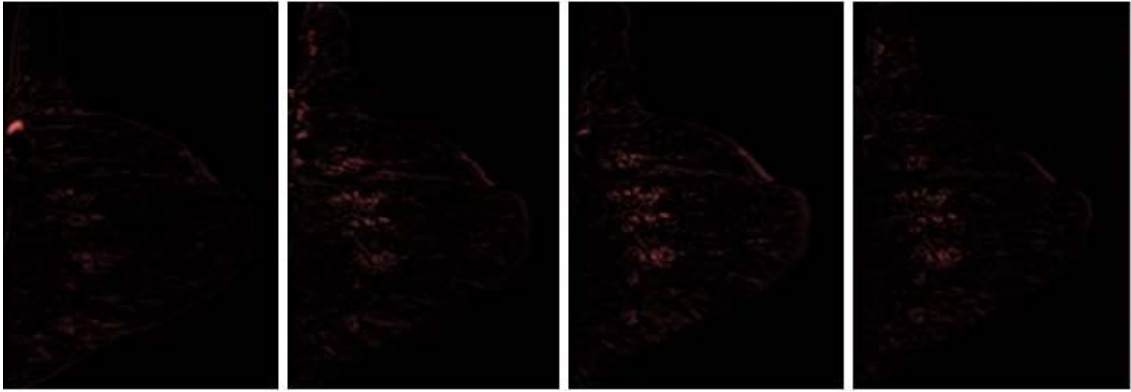
Figure 3.10: Difference images between 2D slices of the 4D CT image acquired during exhalation and its corresponding image simulated using the Marlow hyperelastic model with variable Poisson's ratio. Left to right correspond to end inhale to end exhale images.
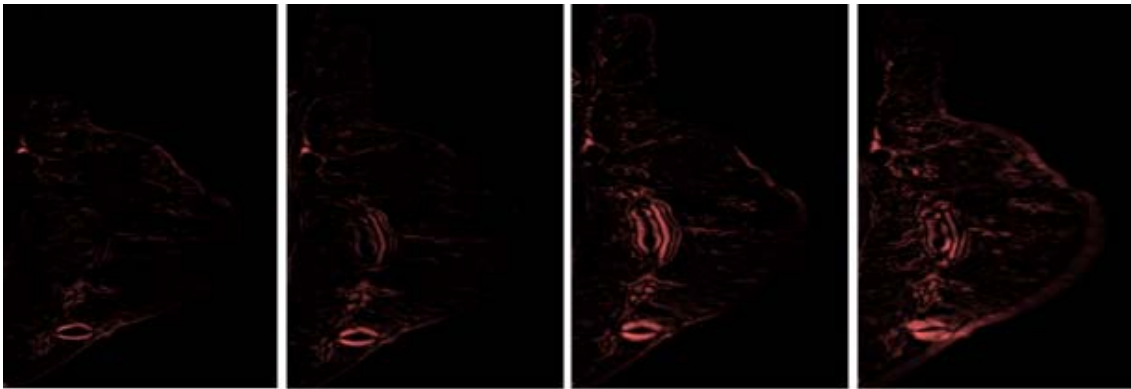
Figure 3.11: Difference images between 2D slices of the 4D CT image acquired during exhalation and its corresponding image simulated using the Marlow hyperelastic model with constant Poisson's ratio. Left to right correspond to end inhale to end exhale images.

3.4. Discussion and Conclusions

This article presents a novel lung biomechanical model where lung tissue incompressibility variation throughout respiration is considered and characterized. While many applications that involve lung tissue biomechanical simulation can benefit from the proposed model, the main purpose pursued in this work is lung tumor motion tracking

during lung cancer treatment with external beam radiation therapy. The proposed biomechanical model utilizes Marlow hyperelastic model or linear elastic model where variable Poisson's ratio is used to characterize tissue incompressibility. Unlike previously proposed models, this model takes into account tissue incompressibility variation throughout respiration. For clinical application of the proposed model, a prerequisite involves utilizing a limited number of fiducial markers placed preoperatively on the patient's chest and tracked during respiration using optical or electromagnetic tracking systems. Motion data of these markers are to be correlated with the patient's diaphragm configuration obtained from 4D CT image sequence. A function can be developed that expresses the diaphragm's configuration with the fiducials coordinates. During radiation therapy treatment, the fiducial markers are placed on the same positions over the chest and tracked using a tracking system. The developed function can be then used to determine the diaphragm's configuration necessary to obtain the prescribed boundary conditions to be input into the proposed lung's biomechanical model to calculate the corresponding tumor location.

Through an in-silico phantom study, we demonstrated that considering tissue incompressibility variation has paramount importance for predicting tumor motion with high accuracy. To complement the proposed lung biomechanical model, we also developed a technique for measuring the tissue's variable Poisson's ratio with linear elastic and Marlow hyperelastic models throughout a respiration cycle. This measurement technique uses the lung's 4D CT image data for this purpose. It follows an optimization framework whereby the Poisson's ratio and pressure in each respiration time point are determined such that the acquired images and their image counterparts constructed using the proposed lung's biomechanical model have maximum similarity. A similar approach was employed to acquire a constant Poisson's ratio in conjunction with the Marlow hyperelastic model throughout a respiration cycle. This was done to demonstrate that using variable incompressibility increases the lung's biomechanical model accuracy. The value of image similarity and difference images between simulated and corresponding acquired images was used to assess the advantage of using variable incompressibility to achieve more realistic results.

Compared with previous models [5,8,9,20,22,27], the proposed model is more consistent with the lung tissue physiological changes during respiration. Moreover, while other proposed techniques ensure lung surface motion consistency with the pleural cavity [5,9], our model also ensures consistency with the lung's volumetric anatomical changes throughout respiration. The latter is critical for predicting highly accurate tumor motion. An ex-vivo porcine animal model was used to test the proposed measurement technique. For this purpose, 4D CT images of the porcine ventilated lung were acquired throughout a respiration cycle. Image data of the inspiration part was used to measure the variable Poisson's ratio. The measured values were validated using image data of the expiration part. Difference images obtained in this validation study indicate that the estimated Poisson's ratio can be reliably used for respiration times both inside and outside of the inspiration phase. The porcine's model pressure variations obtained from the optimization technique are similar to variations reported in the literature [25,29]. Difference images of selected slices and incremental cost function values indicate desirable accuracy of the measured variable Poisson's ratio and pressure values. It is expected that more accurate tissue hyperelastic parameters which are more characteristic of tissue tension behavior lead to higher image similarity, hence further improved accuracy.

The proposed technique can be used in-vivo for patient specific Poisson's ratio measurement. For this purpose, a 4D CT image set of the patient's lung routinely acquired preoperatively can be used. In this case, realistic boundary conditions can be delineated from the images hence more realistic contact model would be required to simulate the chest wall and diaphragm effects. Our future research plans involve in-vivo lung model development and tissue incompressibility characterization. However, to be able to utilize respiratory system FE modeling for real-time tumor tracking, particularly with hyperelastic materials assumption and high resolution FE mesh which are necessary for accurate modeling, the major problem is the excessive amount of time required for FE analysis. To accelerate the FE analysis and facilitate real-time tumor location updating, it is feasible to employ statistical FEM (SFEM) or GPU programming [36,37]. Using these methods, the FE results can be obtained in real-time manner paving the way for intraoperative tumor motion estimation. While the computation time required by the

SFEM or GPU models is typically a small fraction of a second which is very small, it may not be negligible in intraoperative tumor tracking applications as a small but significant phase lag is expected between the updated tumor location and its actual counterpart. This lag can be considered using a data sequence of tumor location, velocity and acceleration over a small time window prior to the current time point. More complex fuzzy logic based algorithms can also be used to compensate for this delay [38].

References

[1] American cancer society, http://www.cancer.org/Research/CancerFactsFigures/index

[2] A. Jemal, F. Bray, M.M. Center, J. Ferlay, E. Ward, D. Forman, "Global cancer statistics," CA Cancer Journal for Clinicians 61, 69-90 (2011).

[3] A.S. Naini, "Modeling lung tissue motions and deformations: Applications in tumor ablative procedures, "Electronic Dissertation Repository 159, http://ir.lib.uwo.ca/etd/159, (2011).

[4] R. Martinez-Monge, C. Garran, I. Vivas, J.M. Lopez-Picazo, "Percutaneous CT-guided 103Pd implantation for the medically inoperable patient with T1N0M0 non-small cell lung cancer: a case report," Brachytherapy 3, 179-181 (2004).

[5] R. Werner, J. Ehrhardt, R. Schmidt, H. Handels, "Patient-specific finite element modeling of respiratory lung motion using 4D CT image data," Med. Phys. 36, 1500-1511 (2009).

[6] M.K. Bucci, A. Bevan, M. Roach 3rd, "Advances in radiation therapy: conventional to 3D, to IMRT, to 4D, and beyond," CA Cancer. J. Clin. 55, 117-134 (2005).

[7] G. Li, D. Citrin, K. Camphausen, B. Mueller, C. Burman, B. Mychalczak, R.W. Miller, Y. Song, "Advances in 4D medical imaging and 4D radiation therapy," Technol. Cancer.Res. Treat. 7, 67-81 (2008).

[8] A. Al-Mayah, J. Moseley, K.K. Brock, "Contact surface and material nonlinearity modeling of human lungs," Phys. Med. Biol. 53, 305-317 (2008).

[9] A. Al-Mayah, J. Moseley, M. Velec, K.K. Brock, "Sliding characteristic and material compressibility of human lung: Parametric study and verification," Med. Phys. 36, 4625-4633 (2009).

[10] M.L. Kessler, "Image registration and data fusion in radiation therapy," Br. J. Radiol. 79 Spec No 1, S99-108 (2006).

[11] W.R. Crum, T. Hartkens, D.L. Hill, "Non-rigid image registration: theory and practice," Br. J. Radiol. 77 Spec No 2, S140-53 (2004).

[12] J.B.A. Maintz and M.A. Viergever, "A survey of medical image registration," Med. Image Anal. 2, 1-36 (1998).

[13] M. Urschler and H. Bischof, "Assessing breathing motion by shape matching of lung and diaphragm surfaces," presented at Physiology, Function, and Structure from Medical Images, SPIE Medical Imaging, 13-15 Feb. 2005.

[14] A. Al-Mayah, J. Moseley, M. Velec, S. Hunter, K. Brock, "Deformable image registration of heterogeneous human lung incorporating the bronchial tree," Med. Phys. 37, 4560-71 (2010).

[15] M. Holden, "A review of geometric transformations for non-rigid body registration," Medical Imaging, IEEE Transactions on 27, 111-128 (2008).

[16] P. Courtis and A. Samani, "Biomechanical registration of prostate images using statistical shape models," presented at Physiology, Function, and Structure from SPIE Medical Images, 12 Feb. 2006.

[17] P. Courtis and A. Samani, "Detecting mechanical abnormalities in prostate tissue using FE-based image registration," presented at 10th Int. Conf. Med. Image Comput. Assist. Interv. (MICCAI), 29 Oct.-2 Nov. 2007.

[18] D. DeCarlo, J. Kaye, D. Metaxas, J.R. Clarke, B. Webber, N. Badler, "Integrating anatomy and physiology for behavior modeling," presented at Medicine meets Virtual Reality III Proceedings, 19-22 Jan. 1995.

[19] T. Zhang, N.P. Orton, T.R. Mackie, B.R. Paliwal, "Technical note: A novel boundary condition using contact elements for finite element deformable image registration," Med. Phys. 31, 2412-2415 (2004).

[20] P.-. Villard, M. Beuve, B. Shariat, V. Baudet, F. Jaillet, "Simulation of lung behaviour with finite elements : Influence of bio-mechanical parameters," presented at 3rd International Conference on Medical Information Visualisation - BioMedical Visualisation, MediVis 2005, London, 5-7 July 2005.

[21] J. Eom, C. Shi, X.G. Xu, S. De, "Modeling respiratory motion for cancer radiation therapy based on patient-specific 4DCT data," Lect. Notes Comput. Sci. 5762 LNCS, 348-355 (2009).

[22] A. Al-Mayah, J. Moseley, M. Velec, K. Brock, "Effect of friction and material compressibility on deformable modeling of human lung," Lect. Notes Comput.Sci.5104 LNCS, 98-106 (2008).

[23] Z. Shirzadi, A.S. Naini, A. Samani, "Lung tumor motion prediction during lung brachytherapy using finite element model," presented atImage-Guided Procedures, Robotic Interventions, and Modeling, SPIE Medical Imaging 5-7 Feb. 2012.

[24] A.S. Naini, R.V. Patel, A. Samani, "Measurement of lung hyperelastic properties using inverse finite element approach," IEEE Transactions on Biomedical Engineering 58, 2852-9 (2011).

[25] A.P. Santhanam, "Modeling, simulation and visualization of 3D lung dynamics," Electronic Dissertation Repository 1301, http://etd.fcla.edu/CF/CFE0001301, (2006).

[26] A.S. Naini, Ting-Yim Lee, R.V. Patel, A. Samani, "Estimation of lung's air volume and its variationsthroughout respiratory CT image sequences," IEEE Transactions onBiomedical Engineering 58, 152-8 (2011).

[27] J. Saade, A.-.Didier, R. Buttin, J.-.Moreau, M. Beuve, B. Shariat, P.-. Villard, "A preliminary study for a biomechanical model of the respiratory system," presented at International Conference on Computer Vision Theory and Applications, 17-21 May 2010.

[28] E. Promayon and P. Baconnier, "A 3D discrete model of the diaphragm and human trunk," ESAIM Proceedings 23, 66-77 (2008).

[29] L. Sherwood, "Human physiology: From cells to systems," Cengage Learning 7, 464-470, (2008).

[30] D.L.G. Hill, P.G. Batchelor, M. Holden, D.J. Hawkes, "Medical image registration," Phys. Med. Biol. 46, 1-45 (2001).

[31] J.C. Lagarias, J.A. Reeds, M.H. Wright, P.E. Wright, "Convergence properties of the Nelder-Mead simplex method in low dimensions," SIAM Journal on Optimization 9, 112-47 (1998).

[32] A.S. Naini, G. Pierce, Ting-Yim Lee, R.V. Patel, A. Samani, "CT image construction of a totally deflated lung using deformable model extrapolation," Med. Phys. 38, 872-83 (2011).

[33] S. Pieper, M. Halle, R. Kikinis, "3D Slicer," presented at 2004 2nd IEEE International Symposium on Biomedical Imaging: Macro to Nano, 15-18 April 2004.

[34] V. Chu and G. Hamarneh, "MATLAB-ITK interface for medical image filtering, segmentation, and registration," presented at Image Processing, SPIE Medical Imaging,13-16 Feb. 2006.

[35] C.A. Glasbey and K.V. Mardia, "A review of image-warping methods," Journal of Applied Statistics 25, 155-171 (1998).

[36] S.R. Mousavi, I. Khalaji, A.S. Naini, K. Raahemifar, A. Samani, "Statistical finite element method for real-time tissue mechanics analysis," Comput. Methods Biomech. Biomed. Engin. 15, 595-608 (2012).

[37] G.R. Joldes, A. Wittek, K. Miller, "Real-time nonlinear finite element computations on GPU Application to neurosurgical simulation," Comput. Methods Appl. Mech. Eng. 199, 3305-3314 (2010)

[38] M. Kakar, H. Nystrom, L.R. Aarup, T.J. Nottrup, D.R. Olsen, "Respiratory motion prediction by using the adaptive neuro fuzzy inference system (ANFIS)," Phys. Med. Biol. 50, 4721-8 (2005).

Chapter 4

Discussion and Conclusions

4.1. Summary and Conclusions

A novel lung tumor tracking technique based on lung tissue biomechanical modeling is proposed in this research. This technique is capable of determining the tumor's location as a function of time during respiration. Continuous tissue deformation and tumor motion is the major problem in lung cancer radiotherapy techniques as they render tumor targeting necessary for effective treatment very difficult. This is true for both external beam radiation therapy and brachytherapy. FE based biomechanical modeling is utilized to calculate the lung tissue deformation field followed by tumor motion trajectory estimation during respiration. The geometry of the lung and surrounding tissues required for 3D FE mesh generation can be extracted from images acquired preoperatively. Boundary conditions including chest wall and diaphragm configuration, however, need to be updated during the procedure. Tracking a number of fiducial markers that can be placed on the patient's chest by optical or electromagnetic tracking systems can be used to provide updated boundary conditions for the respiratory system FE model in each moment of the procedure. While the tumor tracking approach proposed in this study can be utilized for tumor tracking in both lung brachytherapy and external beam radiation therapy, the biomechanics problems involved in these applications are different as described below.

4.1.1. Chapter 2: Lung Tumor Motion Prediction during Lung Brachytherapy

In this chapter, the proposed tumor tracking technique is employed to estimate a deflated lung's tumor motion. This technique involves the lung's biomechanical model developed using FEM. To minimize tissue deformation during brachytherapy, the target lung is deflated by blocking its main airway. The diaphragm displacement as a result of the other lung breathing, however, exists which causes substantial tissue deformation leading to significant tumor motion. Therefore, the diaphragm motion was applied to the deflated lung's FE model as a prescribed displacement boundary condition while the lung-chest cavity contact problem was not considered as the deflated lung's volume is significantly smaller than the chest cavity volume. With known boundary conditions pertaining to the diaphragm's motion, the tumor's motion trajectory components can be calculated over respiration time. As such, if the diaphragm's configuration can be determined intraoperatively, tumor's position can be identified. To assess the performance of the proposed technique, an ex-vivo porcine lung experiment was conducted. In this experiment, the lung was deflated and loaded in a similar manner to a diaphragm loading. The experimental results of the tumor motion showed a reasonable agreement with the results obtained from the lung's FE model. Moreover, sensitivity analysis performed in-silico confirmed the robustness of the abovementioned technique to estimate deflated lung tumor motion as the motion trajectory did not change significantly as a result of 20% variation of the lung tissue hyperelastic parameters. Therefore, this investigation confirms the suitability of the proposed technique for tumor tracking during seed placement procedure for lung brachytherapy treatment. We believe that using this technique results in minimum deviation from the dosimetry plan and it can help making the brachytherapy treatment possible for lung cancer therapy.

4.1.2. Chapter 3: Towards in-vivo Lung's Tissue Incompressibility Characterization for Tumor Motion Predication during Lung Cancer Radiotherapy

In this chapter, lung tissue deformation and tumor motion which occur during normal respiration is investigated using the proposed technique. In this application, the lung is not deflated and its volume changes continuously while breathing. To model the lung in this case, a biomechanical model was proposed where the lung and surrounding anatomy was modeled using FEM. Negative pressure was applied to the lung surface model in the exhale phase to simulate the lung's loading throughout respiration. Frictionless contact problem was considered between the chest cavity and lung surface. For normal respiration modeling, the lung tissue incompressibility is expected to vary significantly throughout breathing as a result of tissue air content variation. Therefore, the significance of considering variable tissue incompressibility was assessed for accurate tumor motion predication. For this purpose, a phantom study was conducted to evaluate the impact of using variable incompressibility parameter over using a constant incompressibility parameter on tumor motion estimation. The results of this in-silico investigation demonstrated the importance of using variable tissue Poisson's ratio for accurate tumor motion estimation. After establishing this importance, an optimization algorithm was developed to obtain a Poisson's ratio function that describes the tissue incompressibility in terms of the time of each respiration cycle. The optimization cost function was defined using image similarity measures as a criterion of consistency between acquired lung images and their corresponding images obtained from the proposed biomechanical model. The function was calculated based on image data pertaining to the inspiration phase. To validate this function, it was input in the lung's respiration model within the expiration phase time window and a sequence of lung simulated images were obtained. These images showed very good agreement with their acquired image counterparts which implied the validity of the experimentally measured Poisson's ratio function for the entire respiration cycle.

To the author's knowledge, while it was demonstrated that the lung tissue incompressibility variation during respiration is very significant and it has substantial impact on tumor motion, none of the previous investigations have considered this variation in their proposed models. The significance of lung tissue incompressibility variation is quite justified since the tissue air content varies remarkably throughout respiration. This study showed that considering tissue incompressibility variation leads to more accurate tumor motion estimation. It is noteworthy that, compared to previous studies, considering variable Poisson's ratio made possible internal anatomical structures consistency between acquired and simulated images beside surface matching between the chest cavity and deformed lung. The internal structure consistency is very important in tumor motion tracking since the tumor is one of the volumetric anatomical structures of the lung tissue. It is evident that utilizing the experimentally obtained Poisson's ratio function leads to more accurate tumor motion estimation. This function is patient specific and it can be calculated preoperatively for each patient before it is incorporated in the respiration system FE model for intraoperative computer assisted radiation delivery. It is believed that the proposed technique can help improve the performance of lung radiotherapy treatment method by minimizing the radiation over/under dosage for the normal tissue and tumor.

4.2. Discussion and Future work

To employ the proposed technique for in-vivo clinical applications, a number of modifications need to be made to the model. The major problem in respiratory system FE modeling, particularly with hyperelastic materials assumption and high resolution FE mesh which are necessary for accurate modeling, is the excessive amount of time required for FE analysis. To accelerate the FE analysis and facilitate real-time tumor location updating, it is feasible to employ statistical FEM (SFEM) [1] or GPU programming [2]. Using these methods, the FE results can be obtained in real-time manner paving the way for intraoperative tumor motion estimation. While the computation time required by the SFEM or GPU models is typically a small fraction of a second which is very small, it may not be negligible in intraoperative tumor tracking applications as a small but significant phase lag is expected between the updated tumor

location and its actual counterpart. This lag can be considered using a data sequence of tumor location, velocity and acceleration over a small time window prior to the current time point. More complex fuzzy logic based algorithms can also be used to compensate for this delay [3]. One of the prerequisites for achieving highly accurate FE simulation is using accurate parameters characterizing tissue stiffness. The present work was based on measurements conducted on a limited number of tissue samples using indentation technique. Given the tension main mode of lung tissue deformation during respiration and the possibility of mechanical behavior asymmetry in tension and compression, it is possible that some accuracy was lost due to this issue. It is noteworthy that part of this accuracy loss was compensated for using the Poisson's ratio function obtained based on the 4D CT image data. To minimize the impact of this issue on tumor motion estimation in clinical applications, hyperelastic parameters of tissue samples resected from lung cancer patients need to be measured using tensile mechanical testing and their average values used for modeling. Another area of research to be tackled is related to interaction between the lung and the diaphragm and the lung and chest cavity. To simulate the diaphragm and chest cavity more realistically, their deformations in each phase of respiration can be extracted from in-vivo4D image sequence of the respiratory system. In this work, it was proposed that the geometry of the diaphragm and chest cavity during the respiration cycle be obtained using 4D CT preoperatively while the configuration of a set of fiducial markers are simultaneously acquired using an optical or electromagnetic tracking system. The image and fiducial markers position sequence data can be combined to obtain a function that provides the chest cavity and diaphragm geometry as a function of time as described in Chapter 1. Further research is required to implement this proposed technique and fine tune it.

This study is the first step of utilizing this technique where its feasibility and fidelity for tumor tracking was demonstrated. Results show that utilizing this approach leads to accurate tumor targeting, hence radiation over/under dose can be reduced for successful and effective lung cancer treatment.

References

[1] S.R. Mousavi, I. Khalaji, A.S. Naini, K. Raahemifar, A. Samani, "Statistical finite element method for real-time tissue mechanics analysis," Comput. Methods Biomech. Biomed. Engin. 15, 595-608 (2012).

[2] G.R. Joldes, A. Wittek, K. Miller, "Real-time nonlinear finite element computations on GPU – Application to neurosurgical simulation," Comput. Methods Appl. Mech. Eng.199, 3305-3314 (2010)

[3] M. Kakar, H. Nystrom, L.R. Aarup, T.J. Nottrup, D.R. Olsen, "Respiratory motion prediction by using the adaptive neuro fuzzy inference system (ANFIS)," Phys. Med. Biol. 50, 4721-8 (2005).

Appendix 1

Permission to reproduce the paper, which has been published under Society for Photo-optical Instrumentation Engineers (SPIE) copy right, in this thesis.

-------- Original Message --------
From: **Scott McNeill**
Date: Jul 19, 2012 11:08:04 AM
Subject: RE: Including my SPIE published paper in the thesis

Dear Zahra Shirzadi,

 Thank you for seeking permission from SPIE to reprint material from our publications. As an author of the cited work, you retain co-owner rights to the original content therein. Publisher's permission is hereby granted under the following conditions: (1) the material to be used has appeared in our publication without credit or acknowledgment to another source; and (2) you credit the original SPIE publication. Include the authors' names, title of paper, volume title, SPIE volume number, and year of publication in your credit statement.

 Sincerely,
 Scott McNeill for
Eric Pepper, Director of Publications
SPIE

-------- Original Message --------
From: **"Zahra Shirzadi"**
Date: Jul 13, 2012 1:59:41 PM
Subject: Including my SPIE published paper in the thesis

Dear Sir/Madam,

 I am writing to get your permission to include my published SPIE paper in my thesis. The thesis is to be submitted in partial fulfillment of the requirements for the degree of Master of Engineering Science to the School of Graduate and Postdoctoral Studies, The University of Western Ontario. The following paper was published by SPIE in 2012:

Z. Shirzadi, A.S. Naini, A. Samani, "Lung tumor motion prediction during lung brachytherapy using finite element model," Proceeding of SPIE Medical Imaging 2012: Image-Guided Procedures, Robotic Interventions, and Modeling, San Diego, California, USA, Vol. 8316, 83160I, 2012.

I am looking forward to hearing from you.

Best Regards,
Zahra Shirzadi,
Graduate Student in Biomedical Engineering program
The University of Western Ontario

Curriculum Vitae

Name:	Zahra Shirzadi

Post-secondary Education and Degrees:

Amirkabir University of Technology
Tehran, Iran
2005-2009 B.Sc., Electrical Engineering

The University of Western Ontario
London, Ontario, Canada
2010-2012 M.Sc., Biomedical Engineering

Honors and Awards:

One of the eight finalists for **Best Student Paper award** at International Society for Photo-optical Instrumentation Engineers **(SPIE) Medical Imaging** 2012

Western Engineering Graduate Scholarship (WES) 2010-2012

Ranked **1st** academically among all Electrical Engineering B.Sc. students Sep. 2009

University Exceptional Students Scholarship, Amirkabir University of Technology 2005-2009

Recognized as **Outstanding student** by Ministry of Science of Iran Sep. 2005

Related Work Experience

Graduate Teaching Assistant for "*Programming Fundamentals*", Department of Electrical and Computer Engineering, The University of Western Ontario, Summer 2012

Graduate Teaching Assistant for "*Programming Fundamentals*", Department of Electrical and Computer Engineering, The University of Western Ontario, Winter 2012

Graduate Teaching Assistant for "*Medical Imaging*", Department of Medical Biophysics, The University of Western Ontario, Fall 2011

Graduate Teaching Assistant for "*Introduction to Electronics*", Department of Electrical and Computer Engineering, The University of Western Ontario, Winter 2011

Publications:

- **Zahra Shirzadi**, Ali Sadeghi Naini and Abbas Samani, "*Lung Tumor Motion Prediction during Lung Brachytherapy Using Finite Element Model*", Proceedings of Society for Photo-optical Instrumentation Engineers (SPIE): Medical imaging 2012, Vol. 8316.

- Ali Sadeghi Naini, **Zahra Shirzadi** and Abbas Samani, "*Modeling Deflated Lung's tumor Motion of Respiratory Contact forces for Minimally Invasive Tumor Ablative Procedures*", under review at IEEE Transactions on Biomedical engineering Journal (TBME) 2011.

- **Zahra Shirzadi** and Abbas Samani, "*Towards in-vivo Lung's Tissue Incompressibility Characterization for Tumor Motion Predication during Lung Cancer Radiotherapy*", submitted at Medical Biophysics Journal.